

RSC Advances



This is an *Accepted Manuscript*, which has been through the Royal Society of Chemistry peer review process and has been accepted for publication.

Accepted Manuscripts are published online shortly after acceptance, before technical editing, formatting and proof reading. Using this free service, authors can make their results available to the community, in citable form, before we publish the edited article. This *Accepted Manuscript* will be replaced by the edited, formatted and paginated article as soon as this is available.

You can find more information about *Accepted Manuscripts* in the [Information for Authors](#).

Please note that technical editing may introduce minor changes to the text and/or graphics, which may alter content. The journal's standard [Terms & Conditions](#) and the [Ethical guidelines](#) still apply. In no event shall the Royal Society of Chemistry be held responsible for any errors or omissions in this *Accepted Manuscript* or any consequences arising from the use of any information it contains.

Cite this: DOI: 10.1039/c0xx00000x

www.rsc.org/xxxxxx

ARTICLE TYPE

Fe(II)_(aq) uptake of Mg(II)-Al(III)/Fe(III)-SO₄/CO₃ HTLCs under alkaline conditions: adsorption and solid state transformation mechanisms

Mario A. Gomez^{*a}, M. Jim Hendry^a, Samir Elouatik^b, Joseph Essilfie-Dughan^a, Susanta Paikaray^b

⁵ Received (in XXX, XXX) Xth XXXXXXXXX 20XX, Accepted Xth XXXXXXXXX 20XX
DOI: 10.1039/b000000x

Abiotic reduction of Mg(II)-Al(III)/Fe(III)-SO₄/CO₃ hydrotalcites (HTLCs) was investigated under three anoxic abiotic reaction conditions: (1) a target pH of 8 and 10 mM Fe(II)_(aq), (2) a target pH of 8 and 0.5 mM Fe(II)_(aq), and (3) a target pH of 10 and 0.5 mM Fe(II)_(aq). Under both Fe(II)_(aq) concentrations and at the targeted pH of 8, the greatest Fe(II)_(aq) uptake, Mg(II)_(aq) release, and least deviation in pH was observed for Fe-based HTLCs (Mg(II)-Fe(III)-SO₄/CO₃) irrespective of the interlayer ion (SO₄ or CO₃). In contrast, the Al-based HTLCs showed the greatest pH drift from the target pH of 8; this phenomenon was attributed to remaining total Fe(II+III) in solution. At the target pH of 10 and 0.5 mM Fe(II)_(aq), the pH of the Al-based HTLCs was greater than the Fe-based HTLCs despite 99% of the Fe(II) being removed from solution in both cases. The greatest Mg(II)_(aq) release was again observed for the Fe-based HTLCs. Unique to these reaction conditions was the readsorption of the released Mg(II)_(aq) by the Mg-Fe-CO₃ HTLC. The major reaction phases produced from the adsorption of Fe(II)_(aq) onto Mg(II)-Al(III)/Fe(III)-SO₄/CO₃ HTLCs were green rust (GR) and magnetite (MG). Two types of phase transformation mechanisms are suggested to occur during the adsorption of Fe(II)_(aq) onto Mg(II)-Al(III)/Fe(III)-SO₄/CO₃ HTLCs, both dependent upon the metal ion (Al vs. Fe) and independent of the interlayer ions (SO₄ or CO₃). For Fe-based HTLCs (Mg-Fe-SO₄/CO₃), surface adsorption of Fe(II)_(aq) and surface precipitation allows electron transfer (between Fe(II)↔Fe(III)) and subsequent atom exchange to occur at the surface as well as within the bulk HTLC structure. For the Al-based HTLCs (Mg-Al-SO₄/CO₃), this surface adsorption of Fe(II)_(aq) and surface precipitation still occur but electron transfer is limited to the precipitated surface phase due to the redox inactivity of the Al(III) groups in the HTLC structure.

Cite this: DOI: 10.1039/c0xx00000x

www.rsc.org/xxxxxx

ARTICLE TYPE**1. Introduction**

Hydrotalcites (HTLCs) are made up of hydroxycarbonates of Mg(II) and Al(III) with the common formulae $Mg_6Al_2(OH)_{16}CO_3 \cdot 4H_2O$. This family of compounds can be described by the general formula $[M(II)_{1-x}M(III)(OH)_2] (A^{n-})_{x/n} \cdot mH_2O$, where M(II) and M(III) are di- or tri-valent metals, A^{n-} is an interlayer anion, and x is the M(III)/M(III)+M(II) ratio. For example, pyroaurite is a variety of HTLC where Fe(III) occurs in the HTLC structure instead of Al(III). Many other cation-anion sequences (e.g., Mg(II) ↔ Co(II), Ni(II), Zn(II), Fe(II), Cu(II), Mn(II), Al(III) ↔ Fe(III), Cr(III) and $CO_3(-II) \leftrightarrow SO_4(-II)$, $NO_3(-I) \leftrightarrow Cl(-I)$) can exist in synthetic or natural systems. Since their discovery in 1842, HTLCs have attracted much attention in many multidisciplinary research fields (such as catalysis, surface science, organic-bio and inorganic synthesis, electrochemistry, mineralogy, soil science, and environmental engineering/science) and been translated into industrial applications (chemical manufacturing, concrete production, pharmaceuticals and Uranium mining companies) because of their: (i) adsorption capacity; (ii) the cation-exchange ability of the brucite layer; (iii) the anion-exchange ability of the interlayer space; (iv) the tunable basicity of the surface, and (v) the control on toxic aqueous metals (e.g., As, Ni, Se) and radio-nucleotides in natural and anthropogenic (e.g., mine tailings) environments.

To date, the dominant research focus has been on improving understanding of the formation mechanism of HTLCs with mixed M(II)-M(III)- A^{n-} ion solutions in compositional varieties (e.g., Ni(II)-Fe(III), Mg(II)-Fe(III), Zn(II)-Al(III), $SO_4(-II)-CO_3(-II)$, $CO_3(-II)-Cl(-I)$) and/or HTLC formation from simple Al(III)/Fe(III) oxides/hydroxides (e.g., $Al(OH)_3$, $Fe(OH)_3$, $AlOOH$, $FeOOH$). To the best of our knowledge, the phase transformation and abiotic anoxic reductive dissolution of HTLC phases under the influence of environmentally important metal ion species (e.g., $Fe(II)_{(aq)}$) under anoxic geochemical conditions is not known. This is in contrast to the well-studied multi-element (e.g., As) control phases, including ferrihydrite (FH) and other Fe-oxy/hydroxides (e.g., lepidocrocite, LP; magnetite, MG; goethite, GT; hematite-HT) or Al-oxy/hydroxides (e.g., gibbsite, GB; alumina, AL). Recently, extended X-ray absorption fine structure (EXAFS) was used to show that Fe(II)-Al(III) layered double hydroxides can be formed at near neutral pH from Al_2O_3 , clay (mica-montmorillonite), and amorphous silicate but not HTLC substrates. Thus, the objectives of this study were to investigate $Fe(II)_{(aq)}$ sorption onto the surface of Mg(II)-Al(III)/Fe(III)- SO_4/CO_3 HTLCs in alkaline abiotic anoxic environments and characterize any Fe(II)-Mg(II)-Al(III)/Fe(III)- SO_4/CO_3 phases that form. An additional objective was to investigate how the metal composition of the HTLC phase (Al ↔ Fe) and interlayer ($SO_4 \leftrightarrow CO_3$) ions affect the type of Fe(II)-

Mg(II)-Al(III)/Fe(III)- SO_4/CO_3 phases formed via different types of formation mechanisms.

2. Experimental**2.1 Synthesis of Mg(II)-Al(III)/Fe(III)- SO_4/CO_3 Hydrotalcites**

Samples of Mg(II)-Al(III)/Fe(III)- SO_4/CO_3 HTLCs were prepared at room temperature (21 °C) using the co-precipitation method. In the case of the $MgAlCO_3$ HTLC, for example, this involved adding a solution (via a peristaltic pump, rate 1000 mL/h) containing $MgCl_2 \cdot 6H_2O$ and $AlCl_3$ (in molar proportions to yield an M(II)/M(III) molar ratio of 2) to a solution containing 3.5 M NaOH and 0.95 M $NaCO_3$ and mixing. The final pH of these solutions from which the solids precipitated was 13.4. In the case of $MgFeCO_3$, $MgAlSO_4$, and $MgFeSO_4$ HTLCs, chemical grade reagents were used following the same procedure as described above.

The wet solids produced by precipitation were washed in deionized water (pH 5.5) five times to remove Cl impurities, then air dried for 24 h at ambient temperature. These solids were then characterized using inductively coupled plasma mass spectrometry (ICP-MS), X-ray diffraction (XRD), and micro-Raman spectroscopy to confirm the Mg(II)-Al(III)/Fe(III)- SO_4/CO_3 HTLC phases (Fig. S1a; Table S0). Dried samples from this batch were transferred to a glove box (UNILab station from MBraun, Germany; 100% N_2) for abiotic reduction tests (discussed below). For comparative purposes, GR, LP, GT, FH, MG, GB, boehmite (Bo: $Al(OH)_3$), Mg(II)-Al(III)-Fe(III) containing- SO_4-CO_3 HTLCs (see Fig. S1b), and amorphous $Al(OH)_3$ were also synthesized using published methods. Reagent grade MgO, $Mg(OH)_2$ (brucite), $MgAl_2O_4$, and $Al_2(SO_4)_3$ from Sigma-Aldrich were also used as reference materials.

2.2 Abiotic batch reactions

Abiotic anoxic Fe(II) redox reactions of Mg(II)-Al(III)/Fe(III)- SO_4/CO_3 HTLCs were conducted in duplicate and in some cases triplicate (for phase confirmation) using $Fe(II)SO_4 \cdot 7H_2O$ (Fisher Scientific) as the $Fe(II)_{(aq)}$ catalyst. $Fe(II)_{(aq)}$ concentrations of 0.5 and 10 mM were chosen for further study (discussed below). The $Fe(II)_{(aq)}$ stock solution was made by dissolving the $Fe(II)SO_4 \cdot 7H_2O$ salt in deoxygenated deionized water (pH ~6) to yield a 10 mM stock solution. Prior to using this stock solution to make the 0.5 mM solution, it was inspected after sitting overnight (12 h) to confirm the absence of any yellow colour (indicative of Fe(II) oxidation). A final confirmation that $Fe(II)_{(aq)}$ was active in solution was done using Fe^{+2} Quant Test Strips (Sigma-Aldrich). The presence of red and the degree of color saturation in the strip is indicative of the Fe^{+2} -cyano complex that forms and the approximate concentration range, respectively; red colour was

confirmed for both the 0.5 and 10 mM solutions and the degree of saturation was greater in the latter case. $\text{Fe(II)}_{(\text{aq})}$ concentrations were inferred from measurements of the total Fe in solution via ICP-MS. In our initial reaction solutions, we assumed the amount of $\text{Fe(II)}_{(\text{aq})}$ and the measured total Fe were the same; the solutions were prepared in the glove box where no Fe(III) was present and pure ferrous sulfate hydrated salt was used as the $\text{Fe(II)}_{(\text{aq})}$ source. In the final solutions from the reactions, both $\text{Fe(III)}_{(\text{aq})}$ and $\text{Fe(II)}_{(\text{aq})}$ could exist due to the dissolution of the $\text{Mg(II)-Al(III)/Fe(III)-SO}_4/\text{CO}_3$ HTLCs and/or lack of total $\text{Fe(II)}_{(\text{aq})}$ adsorption; thus, $\text{Fe(II)}_{(\text{aq})}$ content could not be assumed from the total Fe content. Preliminary tests conducted using only the aqueous Fe(II) solutions (no $\text{Mg(II)-Al(III)/Fe(III)-SO}_4/\text{CO}_3$ HTLC solids) demonstrated the formation of undesirable precipitates (likely $\text{Fe(OH)}_{2(\text{s})}$) at concentrations >10 mM $\text{Fe(II)}_{(\text{aq})}$ at pH 8 and >0.5 mM $\text{Fe(II)}_{(\text{aq})}$ at pH 10 (Fig. S2). As such, subsequent experiments were only conducted at $\text{Fe(II)}_{(\text{aq})}$ concentrations of 0.5 and 10 mM at pH 8 and 0.5 mM at pH 10. These pH values can be typical of natural and anthropogenic (e.g., mine tailings) environments but do not include the lower and neutral pH ranges.

The $\text{Mg(II)-Al(III)/Fe(III)-SO}_4/\text{CO}_3$ HTLCs, $\text{Fe(II)SO}_4 \cdot 7\text{H}_2\text{O}$, and Ca(OH)_2 (Sigma-Aldrich) as well as deoxygenated-deionized water (produced by bubbling with $\text{N}_2(\text{g})$ for 2 h) were placed in the glove box for 3 d to scrub adsorbed or dissolved oxygen from solids or solutions prior to use. After this 3 d period, saturated lime water (our base) was created in the glove box by dissolving 10 g of solid reagent grade Ca(OH)_2 (Sigma-Aldrich) in 1000 mL of the deoxygenated deionized water. To create the test solutions, 40 mL of the $\text{Fe(II)}_{(\text{aq})}$ solution were transferred into 150 mL glass beakers, the pH adjusted with the lime water to the target pH (8 or 10 ± 0.1), and 400 mg of the desired $\text{Mg(II)-Al(III)/Fe(III)-SO}_4/\text{CO}_3$ HTLC solid then added. The pH was again measured and adjusted each day (if necessary) of the 7 d reaction period to maintain the target pH of 8 or 10. The reactions were allowed to proceed for 7 d to ensure completion of the reduction reactions and to emulate a Toxicity Characteristic Leaching Procedure (TCLP)-like leachability test on Fe, Al, and Mg.⁴³ Similar reactions for $\text{Fe(III)/Al(III)-oxide/hydroxides}$ occur in hours^{30, 42} and, as such, a 7-d period was considered sufficient for our purposes. Reported pH ranges are the mean of duplicate tests.

One mL of aqueous sample was collected from each reaction vessel using a 10-cm³ syringe with a 0.02 μm filter (Whatman Inc.) on day 1, 2, 4, and 7 of the experiment and analyzed for total Fe, Mg, and Al via ICP-MS. All solution data reported here represent the total element concentration and are not partitioned into the possible redox states that may occur in solution (e.g., Fe(II) and Fe(III)). Concentrations or percentages reported for elements of interest in solution represent the mean of duplicate tests. After aqueous sample collection on day 7, the remaining solution was separated from the solid via decantation and the solid left inside the glove box to dry. Solids samples were then powdered using a mortar and pestle in the glove box and subsamples collected and stored for analysis using the elemental, molecular, and structural techniques described below. All experiments were conducted at ambient temperature.

Separate reactions at a target pH of 8 and 10 mM $\text{Fe(II)}_{(\text{aq})}$ were

conducted on the $\text{Mg(II)-Al(III)/Fe(III)-SO}_4/\text{CO}_3$ HTLCs and stopped after day 1 of the reaction period to characterize the solids in detail and the mechanism of formation of the reacted phases observed after day 7.

2.3 Analytical Methods

Ambient X-ray diffraction and inert atmosphere ($\text{N}_2(\text{g})$) micro-Raman spectroscopic analyses were conducted on the initial and final (day 7) reacted solids ($\text{Mg(II)-Al(III)/Fe(III)-SO}_4/\text{CO}_3$ HTLCs). For XRD measurements, methanol (600 μL) was added to the ground dried powder subsamples to create a thin paste. This paste was then dropped onto a flat glass sample holder, evenly distributed, and allowed to dry. Measurements were conducted using a PANalytical Empyrean instrument with a rotating anode (2.7 kW) and a Co target (λ Co $K_{\alpha} = 1.7902$ Å) using a graphite monochromator, operating at 40 kV and 45 mA. Scanning took place between 10 and 80 deg 2θ with a 0.01 deg step and scan step time of 85 s. All XRD measurements were collected under ambient conditions as no inert environment cell was available. Phase detection limits for lab-based XRD generally range from 1-5 wt.%.⁴⁴

Phase identification was conducted using the Phase-ID function in X^{pert} HighScore Plus software and the corresponding Joint Committee on Power Diffraction Standards (JCPDS) database reference data for FH (PDF 98-007-6750 and 98-011-1017), LP (PDF 98-001-2041), GT (PDF 98-003-4786), MG (98-011-7729), fougierite/ GR(CO_3) (PDF 98-011-2393), and HT (PDF 98-011-9589). In addition, XRD analyses were conducted on commercial reagent grade GT (CAS No. 1310-14-1), LP (CAS No. 12022-37-6), and MG (CAS No. 1309-38-2).

Inert atmosphere micro-Raman spectroscopic analysis was conducted using a Renishaw InVia Raman microscope equipped with a polarized argon laser operating at 785 nm. The laser delivered 25 mW at the laser exit and 8 mW at the sample using the 20x long distance objective (pot size of ~ 1 μm). Reacted samples as well as air-sensitive reference samples remained under inert anoxic conditions by placing them inside the Renishaw THMS 600 hot-cold cell with $\text{N}_2(\text{g})$ sparged continuously during data collection at 25 °C (Fig. S3a). The high quality of the inert atmosphere Raman data was confirmed by the quality of data for our synthetic GR in comparison to literature Raman data.^{45, 46}

Five scans were collected from 150 to 1400 cm^{-1} and the average taken to improve the resolution and the statistics of the collected data; some data remained noisy irrespective of how many scans were taken or the duration of time over which they were acquired. The energy resolution was 4 cm^{-1} at the full width half maximum of the internal Si reference peak. The scans were collected at 10% of the laser output at the microscope exit to minimize radiation damage or local induced heat transformation of FH to HT or MG.⁴⁷

The system was calibrated to the 520 cm^{-1} Si peak (for position and intensity) before data collection. Phase detection limits for micro-Raman are typically on the order of 1 wt.%.⁴⁸ Data collection and spectral treatment were performed with WiRE 2.0 software from Renishaw. For all samples, three to five random areas were probed to ensure that the phase(s) were consistent throughout the sample. The Raman data presented represent two spectra from the various spots probed in the final reacted 7 d samples that reflect the mixture of phases found throughout the reacted sample. Additional inert Raman data were collected on

the reacted Mg(II)-Al(III)/Fe(III)-SO₄/CO₃ HTLCs at a target pH of 8, Fe(II)_(aq) concentration of 10 mM, and after 1 day of reaction time.

Fe L-edge, Mg K-edge, and Al K-edge inert atmosphere X-ray absorption near edge structure (XANES) spectra were collected at the Canadian Light Source (CLS) on the spherical grating monochromator (SGM)⁴⁹ 11ID-1 beamline ($\Delta E/E$: $\sim 10^{-4}$). To ensure our samples remained under anoxic conditions during testing, all powders (reacted and reference samples) were pressed onto carbon tape inside an anaerobic (N₂(g)) glove box attached to the SGM X-ray absorption end station (Fig. S3b). XANES spectra were recorded using the medium and high energy gratings along with the surface sensitive total electron yield (TEY) and bulk sensitive fluorescence yield (PFY) detectors under high vacuum (5×10^{-8} Torr). The entrance and exit slits were set at $50 \times 50 \mu\text{m}$. Note that the raw un-calibrated energy XANES data are presented in the text for relative energy comparison purposes whereas the energy calibrated data are presented in the supplementary information. The energy calibration was accounted for in our work to ensure that any shifts in the energy of the XANES data being interpreted were real and not due to beamline energy differences of samples analyzed on different dates (which at SGM-CLS can be up to ~ 1 eV). Fe L-edge spectra were normalized using a single normalization method and the energy scale of our compounds calibrated to the main L₃ peak of ferrihydrite occurring at 710.5 eV.⁵⁰ Fe L-edge spectra were obtained from 696 to 740 eV using a coarse step size of 0.5 eV before the first edge and a smaller step of 0.1 eV at the main absorption edge(s). The same procedure and step size were followed for the Mg and Al K-edges but using energy ranges of 1290 to 1355 eV and 1555 to 1610 eV, respectively. Because the standards and reacted samples were run on different dates, the Al K-edge of AlSO₄, AlOOH, AlOH₃(GB), and AlOOH (Bo) were calibrated to the first intense peak of boehmite (AlOOH) at 1567.8 eV.⁵¹ Al K-edges of the reacted samples and Mg(II)-Al(III)-Fe(III) containing-SO₄-CO₃ HTLC standard were calibrated to the first intense peak of Mg-Al-CO₃ HTLC at 1567.7 eV.⁵¹ Similarly, the Mg K-edges of the MgOH₂, MgO, and MgAl₂O₄ standards were calibrated to the first intense peak of MgO at 1296.9⁵², and the reacted samples and the Mg(II)-Al(III)-Fe(III) containing-SO₄-CO₃ HTLC standard were calibrated to the first peak of Mg-Al-CO₃ HTLC at 1310.0 eV.⁵³ To determine if the oxidation/redox and coordination states at the local Fe, Mg, and Al molecular environments of the reacted Mg(II)-Al(III)/Fe(III)-SO₄/CO₃ HTLCs changed⁵²⁻⁶⁴, the Mg(II)-Al(III)/Fe(III)-SO₄/CO₃ HTLC reacted at the target pH of 8, for 7 d, and using 10 mM Fe(II)_(aq) were analyzed using XANES surface (total electron yield, TEY) and bulk (fluorescence yield, FY; as partial fluorescence yield, PFY) sensitive analysis at the Fe L-edge, Mg K-edge, and Al K-edge. TEY is more surface sensitive than FY (even as PFY) because the sampling depth of TEY is ~ 5 -10 nm from the surface whereas that of FY is deep inside the bulk (≥ 50 nm) of the solids.^{65, 66}

This local sub-micron detection of elements of interest (e.g., Fe, Al, Mg) cannot be achieved by bulk micro techniques such as micro-Raman and XRD due to their inherently longer range wave probes and micro-scale penetration depths.

Bulk elemental analysis of all aqueous and solid samples was

conducted using a Perkin-Elmer NexION 300D ICP-MS instrument with a relative standard deviation (RSD) of $\pm 10\%$. Solid samples were digested in an acidic media (HF-HNO₃), left overnight (12 h) to dissolve, and diluted accordingly for analysis of total Fe, Al, and Mg.^{67, 68} All concentrations or percentages reported represent the mean of duplicate tests. For all tests, the Al leachability throughout the 7 d reaction period was always ≤ 0.3 mg/L (i.e., $< 0.002\%$ of Al dissolved). As a result, Al leachability was deemed unimportant and is not discussed further. The percentage of Mg(II)_(aq) released into solution from the solid and the remaining amount in the solid ($100\% - \text{Mg(II)}_{\text{(aq)}}$ released) were calculated from the average greatest concentration of Mg(II)_(aq) released in the solution for the 7-d period and the initial amount of Mg(II) in the solid (Tables S0-S3). A similar computation was performed for the percent Fe(II)_(aq) remaining in solution after the 7-d reaction period (Tables S1-S3). Individual leachability data for all reaction conditions investigated are available in the supplementary information (Tables S4-S6).

3. Results and Discussion

This section outlines the 7-d reaction behavior in terms of pH, total Fe adsorption, and Mg release as well as phase transformation characteristics of the Mg-Fe-CO₃, Mg-Al-CO₃, Mg-Fe-SO₄, and Mg-Al-SO₄ HTLCs under the three reaction conditions: a target pH of 8 and 10 mM Fe(II)_(aq) [§3.1], a target pH of 8 and 0.5 mM Fe(II)_(aq) [§3.2], and a target pH of 10 and 0.5 mM Fe(II)_(aq) [§3.3]. We further probe the HTLCs via inert XANES analysis under the most aggressive phase changing conditions: a target pH of 8, 10 mM Fe(II)_(aq), and a 7-d reaction time [§3.4]. Finally, we discuss the phase transformation mechanisms that arise as a result of the Fe(II)_(aq) uptake [§3.5].

3.1 Reactions at pH 8 using 10 mM Fe(II)_(aq)

In the reaction vessel containing only Mg-Fe-CO₃ HTLC, the pH increased from the target of 8, resulting in an average pH range of 8.0 to 8.9 throughout the experiment (Fig. 1a). The majority (98%) of the total Fe concentration in solution (as Fe(II)_(aq)) was removed within the first day of the reaction period; by day 7, an average of 99% had been removed (Fig. 1b and Table S1). Mg(II)_(aq) release (similar to the Fe(II)_(aq) uptake) was almost complete after the first day of reaction, increasing slightly during day 2 before remaining constant to the end of the reaction period. A total of 1.42% of the Mg(II) present in the initial solids was released into solution by day 7 (Fig. 1c). Powder XRD data and phase analysis using X'pert Highscore of the reacted greenish Mg-Fe-CO₃ HTLC solid phase at day 7 (Figs. 2 and S4) indicated a considerable mass of unreacted Mg-Fe-CO₃ HTLC as well as the presence of MG, GR, GT, LP, and lesser amounts of FH (always $\leq 5\%$ within the error of the search match). Inert atmosphere micro-Raman analysis (Figs. 2 and S5) confirmed the presence of GR, MG, and the remaining Mg-Fe-CO₃ HTLC. The presence of a GR phase was supported by Raman spectra that showed typical Fe⁺²-O and Fe⁺³-O stretches at 400-500 cm⁻¹; MG was evident by the presence of a band at 665 cm⁻¹.^{45, 46} The pH range measured here for the formation of GR and MG (8.0-8.9) is consistent with literature values for Fe-oxy/hydroxides.^{45, 46, 69, 70}

This observed pH range is important because it provides a pH formation range for Mg(II)-Al(III)/Fe(III)-SO₄/CO₃ HTLC

structures that have been unknown to date and demonstrates another family of structures from which GR and MG can precipitate.

For the Mg-Al-CO₃ HTLC, the pH deviated from the target of 8 (Fig. 1a and Table S1), but to a lesser extent than its Fe counterpart (Mg-Fe-CO₃) discussed above. Although the final Fe(II)_(aq) removal efficiency (at the end of the reaction period) was 99%, the amount of Fe(total) remaining in solution after the reaction period for Mg-Al-CO₃ was greater than observed for Mg-Fe-CO₃ (Fig. 1b). The relative amount of Mg(II)_(aq) released was only 0.3% by day 7 (Fig. 1c) despite a significant amount of Fe(II)_(aq) being removed from solution onto the Mg-Al-CO₃ HTLC. The reason for the high Fe(II)_(aq) removal and low corresponding release of Mg(II)_(aq) observed under this reacting condition for the Mg-Al-CO₃ is not known. The Mg(II)_(aq) release behavior for the Mg-Al-CO₃ HTLC differed from the Fe-based HTLC counterpart, with substantially less (64 vs. 343 mg/L at 7 days) Mg(II)_(aq) released into solution (Fig. 1c and Table S1). Powder XRD of the final light green solids (Fig. S4) was dominated by the presence of the remaining Mg-Al-CO₃ HTLC (Fig. 2). X³pert HighScore phase analysis showed the presence of MG, GR, GT, LP, and lesser amounts of FH. These phases were less obvious than in the Mg-Fe-CO₃ HTLC counterpart. Micro-Raman analysis of the reacted samples showed the remaining unreacted Mg-Al-CO₃ HTLC but also the presence of GR (Figs. 2 and S5). In this case, the GR phase was identified from an additional SO₄ band in the reacted sample of the Mg-Al-CO₃ HTLC that was not present in the starting material (Figs. 2 and S5). We attribute our observation of a GR(SO₄) type as part of the reacted Mg-Al-CO₃ HTLC product to our reacting Fe(II)_(aq) solution being derived from a soluble sulfate salt (Fe(II)SO₄·7H₂O). Moreover, the inert micro-Raman data contained additional CO₃ bands not derived from the starting Mg-Al-CO₃ HTLC. We attribute this to the presence of a GR(CO₃) phase (i.e., GR with CO₃ and SO₄ in the interlayer).

As observed in the Fe-based carbonate HTLC, the pH increased from the target of 8 to 8.2-8.9 for the Mg-Fe-SO₄ HTLC (Fig. 1a and Table S1). Most of the Fe(II)_(aq) was removed from solution by day 1, with 99% removed by day 7 (Fig. 1b). The total Mg(II)_(aq) released into solution was 1.36% (Fig. 1c and Table S1). The Mg(II)_(aq) release mostly occurred within the first day of reaction and slightly increased to a constant concentration by the end of the reaction period. This observation was consistent with its carbonate counterpart Mg-Fe-CO₃. Powder XRD analyses showed the presence of the remaining unreacted HTLC as well as additional MG peaks (Fig. 2). A phase analysis search showed the presence of MG, GR, GT, LP, and lesser amounts of FH (always ≤ 5%). Inert micro-Raman analysis of the blue-greenish (Figs. 2 and S5) Mg-Fe-SO₄ HTLC solids showed the presence of GR and MG (again, similar to its Fe carbonate counterpart). Literature values for the pH of formation for GR and MG were within our measured average range of 8.2-8.9 based on available Fe-oxo/hydroxide data^{45, 46, 69, 70} and are consistent with the Mg-Fe-CO₃ HTLC data above.

Finally, the measured average pH range for the Mg-Al-SO₄ HTLC (7.5 to 7.7) was the lowest with respect to the target of 8 and the other HTLCs tested (Fig. 1a and Table S1). The amount of Fe(II)_(aq) removed from solution for the Mg-Al-SO₄ HTLC was

also the lowest (81%) observed over the course of the 7 day experiment (Fig. 1b). Notably, in the case of the Mg-Fe-SO₄ HTLC, the majority (99%) of the Fe(II)_(aq) was removed from solution and the pH never fell below 8. As such, the decrease in pH observed in our reactions is attributed to the remaining Fe in solution forming acidic protonated aqueous Fe-SO₄ complexes.⁷¹ Further evidence of this comes from a comparison of the Mg-Al-CO₃ and Mg-Al-SO₄ HTLCs; little to no Fe exists in solution to form these acidic aqueous Fe-SO₄ complexes in the former and, as a result, the pH throughout the reaction period is ~8 or above (Fig. 1 and Table S1). The Mg(II)_(aq) release (0.2 %) from the Mg-Al-SO₄ HTLC was similar to its carbonate counterpart; this indicates that although the Fe(II)_(aq) uptake can be large (99% for Mg-Al-CO₃ and 81% for Mg-Al-SO₄), the corresponding Mg(II)_(aq) release for the Al-based HTLCs (CO₃ or SO₄) is low compared to the Fe-based HTLCs (CO₃ or SO₄). It is noted that although the Mg(II)_(aq) release for the Al-based HTLCs (CO₃ or SO₄) is similar (0.2-0.3 %, see Fig. 1c and Table S1), in the case of the MgAlSO₄ here, the low Fe(II)_(aq) removal (81 %) maybe one reason for the observed low Mg(II)_(aq) release. The Mg-Al-SO₄ solids at the end of the reaction period took on a darker-bluish-green color on the surface than the lighter green solids observed for the Mg-Al-CO₃ HTLC (Fig. S4). XRD analysis of samples from the end of the 7 day reaction period showed the presence of the remaining Mg-Al-SO₄ HTLC but also an additional shoulder at 40° from MG (Fig. 2). Our XRD phase search again indicated the presence of MG, GR, GT, LP, and lesser amounts of FH in our reacted sample. Inert atmosphere micro-Raman analysis of the reacted samples showed the remaining unreacted Mg-Al-SO₄ HTLC but also the presence of GR from the additional SO₄ band (Figs. 2 and S5) not present in the starting Mg-Al-SO₄ HTLC.

3.2 Reactions at a target pH of 8 using 0.5 mM Fe(II)_(aq)

Tests discussed in this section used “trace” Fe(II)_(aq) concentrations (0.5 mM). The lower concentrations of Fe(II)_(aq) ions in solution resulted in a total Fe (as Fe(II)_(aq)) uptake of 99% by all of the solid Mg(II)-Al(III)/Fe(III)-SO₄/CO₃ HTLCs after day 1, and this was maintained to the end of the 7-d reaction period.

For the Mg-Fe-CO₃ HTLC, the measured average reaction pH was greater than the target of 8 and ranged from 9.0 to 9.1 (Fig. 3a and Table S2). Mg(II)_(aq) release into solution was 0.21%, which is almost an order of magnitude less than for 10 mM Fe(II)_(aq) (1.42 %) despite both conditions yielding a 99% Fe(II)_(aq) uptake (Figs. 2b-2c, 3b-3c and Tables S1-S2). The difference in Mg(II)_(aq) release was attributed to fewer Fe(II)_(aq) ions available to exchange with the surface Mg(II) ions of the Mg-Fe-CO₃ HTLC solids under trace Fe(II)_(aq) conditions (Fig. 3b). This is in contrast to tests conducted at 10 mM in which more Fe(II)_(aq) ions were available to exchange with the surface Mg(II) groups of the Mg-Fe-CO₃ HTLC (Figs. 2 and 3). Phase analysis of the reacted Mg-Fe-CO₃ HTLC using XRD and inert micro-Raman spectroscopy (Fig. 4) was dominated by the presence of the remaining Mg-Fe-CO₃ HTLC, but an XRD peak at 35° suggested the presence of MG. Phase analysis via X³pert HighScore indicated the presence of unreacted Mg-Fe-CO₃ HTLC along with MG, GT, LP, and FH (≤ 5 %).

The greatest pH deviation from the target of 8 using trace $\text{Fe(II)}_{(\text{aq})}$ was observed for the Mg-Al- CO_3 HTLC (average pH 9.0 to 9.7; Fig. 3a and Table S2). Consistent with the tests employing 10 mM $\text{Fe(II)}_{(\text{aq})}$ and Mg-Al- CO_3 HTLC, little to no $\text{Mg(II)}_{(\text{aq})}$ was released into solution. The order of magnitude lower release of $\text{Mg(II)}_{(\text{aq})}$ (Fig. 3b-3c and Table S2) under trace $\text{Fe(II)}_{(\text{aq})}$ conditions was also attributed to fewer ions available for exchange with surface Mg(II) of Mg-Al- CO_3 HTLC. However, the $\text{Mg(II)}_{(\text{aq})}$ release was always lower for Mg-Al- CO_3 versus its Mg-Fe- CO_3 counterpart for $\text{Fe(II)}_{(\text{aq})}$ concentrations of both 0.5 and 10 mM. XRD and inert micro-Raman analysis (Fig. 4) of the final Mg-Al- CO_3 HTLC only showed the presence of unreacted Mg-Al- CO_3 HTLC with no evidence of any other common phases (e.g., MG, GR). Phase analysis with X'pert HighScore indicated the presence of MG, GT, LP, and FH but these were less evident than in the Mg-Fe- CO_3 HTLC counterpart. This lack of sensitivity in the macro-bulk (XRD and micro-Raman) analysis was attributed to the small amount of $\text{Fe(II)-Fe(III)-SO}_4/\text{CO}_3$ phases that formed under trace $\text{Fe(II)}_{(\text{aq})}$ conditions. In future studies, nano-techniques such as transmission electron microscopy (TEM)³⁵ will be used to confirm these phase transformations.

In the case of the Mg-Fe- SO_4 HTLC, the measured average pH range was 9.0 to 9.5 and 0.44 % of $\text{Mg(II)}_{(\text{aq})}$ was released into solution by the end of day 7 (Fig. 3 and Table S2). This behavior is very similar to its Mg-Fe- CO_3 HTLC counterpart. Again, powder XRD and micro-Raman data showed only the presence of the remaining unreacted Mg-Fe- SO_4 HTLC.

For the Mg-Al- SO_4 HTLC (Fig. 3 and Table S2), the pH increased from 9.0 to 9.2 under trace $\text{Fe(II)}_{(\text{aq})}$ conditions; this is in contrast to its behavior at high $\text{Fe(II)}_{(\text{aq})}$ concentrations (10 mM), where it exhibited the greatest pH drift (to lower values) compared to all other HTLCs tested. After the 7 d reaction period, 0.02% of the $\text{Mg(II)}_{(\text{aq})}$ was released from the reacted solid. This was one order of magnitude less than its Fe counterpart (Mg-Fe- SO_4) but similar to its CO_3 equivalent (Mg-Al- CO_3) under the same reaction conditions. Powder XRD of the reacted sample was dominated by the presence of the remaining Mg-Al- SO_4 HTLC (Fig. 4). In addition, MG peaks at 35° (weak shoulder) and 41° (shoulder) were detected. X'pert HighScore analyses indicated the presence of unreacted Mg-Al- SO_4 HTLC, MG, GT, LP, and FH ($\leq 5\%$) whereas inert micro-Raman analysis of the final reacted product showed only the presence of the unreacted Mg-Al- SO_4 HTLC.

3.3 Reactions at a target pH of 10 using 0.5 mM $\text{Fe(II)}_{(\text{aq})}$

At the target pH of 10 and 0.5 mM (trace) concentrations of $\text{Fe(II)}_{(\text{aq})}$, the solid Mg(II)-Al(III)/Fe(III)- SO_4/CO_3 HTLCs tested removed 99% of the initial $\text{Fe(II)}_{(\text{aq})}$ during day 1 of the reaction period with no additional release by the end of day 7. These observations were consistent with those at the target pH of 8 and trace $\text{Fe(II)}_{(\text{aq})}$.

The measured average reaction pH for the Mg-Fe- CO_3 HTLC was below the target pH of 10 and ranged from 9.2 to 9.7 (Fig. 5a and Table S3) along with complete $\text{Fe(II)}_{(\text{aq})}$ removal (Fig. 5b). $\text{Mg(II)}_{(\text{aq})}$ release into solution was almost complete during day 1 of reaction (0.1%) after which it was removed (i.e., reabsorbed by the reacted solid) to the end of day 7 (Fig. 5c). Approximately 10 times the mass released into solution on day 1 was adsorbed back

onto the solid at later times. This $\text{Mg(II)}_{(\text{aq})}$ reabsorption behavior was not observed in any other test conducted. The XRD and inert micro-Raman data from day 7 only show the presence of the remaining unreacted Mg-Fe- CO_3 HTLC (Fig. 6). These analyses were not sensitive enough to show phase transformation to other minerals (e.g., MG, GR), likely due to the small amount of $\text{Fe(II)-Fe(III)-SO}_4/\text{CO}_3$ phases formed under 0.5 versus 10 mM $\text{Fe(II)}_{(\text{aq})}$ conditions regardless of pH.

For the Mg-Al- CO_3 HTLC (Fig. 5 and Table S3), the average measured reaction pH ranged from 9.9 to 10.0. As also observed at the target pH of 8 and 0.5 mM $\text{Fe(II)}_{(\text{aq})}$, Fe removal efficiency was 99% for the Mg-Al- CO_3 HTLC at a target pH of 10; in addition, the corresponding $\text{Mg(II)}_{(\text{aq})}$ release was again substantially less for the Mg-Al- CO_3 HTLC than its Mg-Fe- CO_3 counterpart.

Similar to the Fe-based carbonate HTLC, the pH decreased from the target pH of 10 to 9.2-9.5 (Fig. 5 and Table S3) in the Mg-Fe- SO_4 HTLC. Again, the decrease in pH was attributed to the remaining Fe in solution forming acidic protonated aqueous Fe-SO_4 complexes. The $\text{Mg(II)}_{(\text{aq})}$ released into solution was greater (0.27 %) for the Mg-Fe- SO_4 HTLC in comparison to its carbonate counterpart. Moreover, the $\text{Mg(II)}_{(\text{aq})}$ released into solution for the Mg-Fe- SO_4 HTLC remained in solution for the duration of the reaction period and was not reabsorbed back onto the reacted solid phase as observed for the carbonate counterpart. Powder XRD analysis (Fig. 6) of the final reacted Mg-Fe- SO_4 HTLC was dominated by the remaining unreacted Mg-Fe- SO_4 HTLC. Similarly, inert micro-Raman analyses of the reacted sample (Fig. 6) showed only the presence of the remaining Mg-Fe- SO_4 HTLC.

Finally, for the Mg-Al- SO_4 HTLC (Fig. 5 and Table S3), the measured average pH (9.7 to 10.1) was close to the target of 10, similar to the carbonate counterpart (Mg-Al- CO_3 HTLC). The pH behavior of the Al HTLC under these more alkaline conditions was again consistent with the suggestion that remaining Fe in solution is the main cause of the pH decrease from the target pH. The $\text{Mg(II)}_{(\text{aq})}$ released in solution from the Mg-Al- SO_4 HTLC was very low to insignificant (0.001 %), analogous to its carbonate equivalent. Both XRD and micro-Raman analysis of the final reacted samples were dominated by the presence of the remaining Mg-Al- SO_4 HTLC (Fig. 6).

3.4 XANES analysis of HTLCs at a target pH of 8 and 10 mM $\text{Fe(II)}_{(\text{aq})}$

The reaction tests described above show that the phase transformation behavior and the corresponding uptake of $\text{Fe(II)}_{(\text{aq})}$ from solution and release of $\text{Mg(II)}_{(\text{aq})}$ into solution from the surface of the HTLCs are a function of pH, $\text{Fe(II)}_{(\text{aq})}$ concentration, and the type of Mg(II)-Al(III)/Fe(III)- SO_4/CO_3 HTLC. The most dramatic change in terms of phase transformation and corresponding uptake of $\text{Fe(II)}_{(\text{aq})}$ and $\text{Mg(II)}_{(\text{aq})}$ release into solution for all Mg(II)-Al(III)/Fe(III)- SO_4/CO_3 HTLCs occurred at a target pH of 8 with 10 mM $\text{Fe(II)}_{(\text{aq})}$ (§3.1). While ~99 % of the $\text{Fe(II)}_{(\text{aq})}$ was removed from solution after day 1 for all of the Mg(II)-Al(III)/Fe(III)- SO_4/CO_3 HTLCs, only solids for the final (day 7) reaction products were characterized. Therefore, we needed to clarify if the observed phase transformation to GR and MG occurred immediately upon removal of $\text{Fe(II)}_{(\text{aq})}$ from solution (after day 1) and if the same

phase(s) remained after day 7. Inert micro-Raman analyses (Fig. 7) show the formation of both GR and MG after day 1 of the reaction period for all Mg(II)-Al(III)/Fe(III)-SO₄/CO₃ HTLCs. This observation suggests that the reaction products form on day 1 and remain stable through to the end of the reaction period.

For the reacted Mg-Fe-SO₄/CO₃ HTLCs, the presence of GR, MG, and unreacted Mg-Fe-SO₄/CO₃ HTLCs was clearly evident from the bulk inert micro-Raman and XRD data. However, such data for the reacted Mg-Al-SO₄/CO₃ HTLCs were less definitive. Macro-bulk techniques (e.g., XRD and micro-Raman) provide data that represent a combination of all phases present within the probing spot of the laser or X-ray source. Therefore, TEY and PFY Fe L-edge XANES were employed to gain insight into the local Fe molecular environment in the Mg(II)-Al(III)/Fe(III)-SO₄/CO₃ HTLCs under abiotic reductive dissolution.

The surface sensitive TEY Fe L-edge of the 7 day reacted Mg-Fe-SO₄/CO₃ HTLCs indicated the presence of Fe(III) and Fe(II) characters, as expected from the combination of GR, MG and unreacted Mg-Fe-SO₄/CO₃ HTLCs (Fig. 8). Moreover, the sharp pre-peak at low energy (~705 eV) typical of an octahedral low spin Fe(III) compound was not present in the reacted Mg-Fe-SO₄/CO₃ HTLCs. These data suggest that the Fe(III) of the reacted Mg-Fe-SO₄/CO₃ HTLCs remains in a paramagnetic high spin state with an octahedral crystal field. Thus, electron repulsions should dominate ligand field effects and a weak field with a small Δ_o should exist. In addition, Fe(III) in the reacted Mg-Fe-SO₄/CO₃ HTLCs should have an anti-ferromagnetic character as observed for hematite. Based on the above observations, the Fe(III) metal-ligand coordination of the reacted Mg-Fe-SO₄/CO₃ HTLCs should remain in a six-fold environment as it does in unreacted HTLCs.

We confirmed the presence of an Fe(II) environment in the reacted samples (as GR), but detailed information on its specific coordination and electronic state could not be determined as readily as for the Fe(III) species based on the Fe L-edge XANES spectral structure. However, the confirmed formation of GR in the reacted Mg-Fe-SO₄/CO₃ HTLCs along with the inert micro-Raman and Fe L-edge TEY XANES data allow us to presume that the Fe(II) cations should have an octahedral hydroxyl coordination as found in the GR (SO₄ and CO₃) crystal structure.

No clear evidence of Fe(II) tetrahedral ions was noted for the Mg-Fe-SO₄/CO₃ HTLC reacted products, as has been observed in CaBaFe₄O₇ mixed-valent transition metal oxides. PFY Fe L-edge XANES measurements (Fig. 8) suggest that the spectra of the reacted Mg-Fe-SO₄/CO₃ HTLCs had more of a Fe(III) character and did not exhibit clear evidence of Fe(II) as noted in the surface sensitive TEY measurements. The Fe(III) character evident in the more bulk range analyses was attributed to the unreacted Mg-Fe(III)-SO₄/CO₃ HTLCs left over at the end of the

reaction period (consistent with the longer range bulk XRD data). Although the macro-bulk (micro-Raman and XRD; Fig. 2) data of the reacted Mg-Al-SO₄/CO₃ HTLCs showed some presence of GR/MG in addition to the unreacted Mg-Al-SO₄/CO₃ HTLCs, evidence of surface Fe(II)-Fe(III)-SO₄/CO₃ phases is required. Fe L-edge TEY measurements show the presence of an Fe phase on these Mg-Al-SO₄/CO₃ HTLCs (Fig. S6). The Fe phase observed for the reacted Mg-Al-SO₄/CO₃ HTLCs exhibited an Fe(III) character as well as some Fe(II) character, similar to that

observed for the reacted Mg-Fe-SO₄/CO₃ HTLCs (Figs. 8 and S6). Finally, reference Fe L-edge XANES spectra of GR are rare despite its wide occurrence. To date, only one report of XANES spectra of GR similar to our surface sensitive TEY measurements has been published with no consideration given to the nature of its bulk structure. From Fig. 8, the bulk spectra of GR is clearly very distinct from its surface TEY counterpart. In particular, the Fe L₃-edge (~708 eV) of the bulk PFY XANES GR spectra exhibited only Fe(III) characteristics while the smaller Fe L₂-edge (~721 eV) showed only Fe(II) characteristics. This suggests that, although the GR surface is rich in Fe(II) characteristics, the bulk of its structure has a mixed Fe(III)-Fe(II) character; this observation has not been reported to date via redox sensitive XANES analysis. The difference in valency characteristics of the bulk and surface may explain the high reactivity and valency exchange properties at the GR surface.

The Mg and Al K-edge of Mg-Al-CO₃ are reported in the literature and these were compared with spectra from our Mg(II)-Al(III)/Fe(III)-SO₄/CO₃ HTLCs reaction products (Fig. 9). The Mg K-edge (Fig. 9a,c) of the reference MgAl₂O₄ sample showed a typical IV-fold Mg(II) coordination environment while our MgO, MgOH₂, and Mg(II)-Al(III)-Fe(III) containing-SO₄-CO₃ HTLCs displayed a typical VI-fold Mg(II) coordination environment. The reacted Mg(II)-Al(III)/Fe(III)-SO₄/CO₃ HTLCs retained their VI-fold coordination and HTLC-like environment in both the surface (TEY, Fig. 9a) and bulk (PFY, Fig. 9c) measurements. However, the highest Mg K-edge peaks in the reacted Mg-Fe-SO₄/CO₃ HTLCs were shifted to lower energy and were sharper than those from the reacted Mg-Al-SO₄/CO₃ HTLCs. This effect is evident in the surface TEY measurements. According to Mg K-edge XANES theory, the absorption at this edge arises from the electron transition from the 1s to 3p orbital and is observed mainly in the near edge. The energy level of Mg 3p in the Mg-O₄ tetrahedron (T_d) is lower than in the Mg-O₆ octahedron (O_h). Furthermore, the energy level of a distorted octahedron becomes greater than a non-distorted O_h octahedron because of broadening and/or splitting of the 3pσ* state. Thus, the Mg K-edge energy position directly reflects the coordination number and/or ionicity (electronic state). As noted above, Mg(II)_(aq) release for the Fe-based HTLCs was substantially greater than for the Al-based HTLCs. Therefore, the changes in Mg K-edge XANES (Fig. 9a-c) of the Al- vs. Fe-based HTLCs were attributed to differences in Mg(II) surface dissolution and Fe(II)_(aq) uptake. The formation of distorted Mg(II) surface sites on the reacted HTLCs is less pronounced for the Fe-based HTLCs (lower energy Mg K-edge) because the HTLC structure balances the Fe(II)_(aq) surface uptake via a corresponding Mg(II)_(aq) release into solution. In the Al-based HTLCs, Fe(II)_(aq) uptake was great (81-99%) but Mg(II) release from the HTLC surface was not sufficient to alleviate the surface stress of the Fe(II)_(aq) uptake. As such, the Mg K-edge of the reacted Mg-Al-SO₄/CO₃ HTLCs was observed at a higher energy. Although similar trends were observed for the bulk PFY Mg K-edge XANES (Fig. 9c), the effects were more obvious in the surface TEY XANES measurements.

Finally, we investigated the Al K-edge XANES of the reacted Mg(II)-Al(III)/Fe(III)-SO₄/CO₃ HTLCs relative to some reference compounds (Fig. 9b,d). Again, our reference

AlOH₃(gibbsite), AlOH₃(amorphous), AlOOH(diaspore), and Mg(II)-Al(III)-Fe(III) containing-SO₄-CO₃ HTLCs showed a typical VI-fold Al(III) coordination environment. Although we present an experimental IV-fold Al(III) coordination spectra for albite (NaAlSi₃O₈), its single sharp peak at lower energies (1566 eV) is recognized and discussed here based on literature data.⁵³⁻⁵⁶

In general, the reacted Mg(II)-Al(III)/Fe(III)-SO₄/CO₃ HTLCs retained their VI-fold Al(III) coordination and HTLC-like environment in both the surface (TEY) and bulk (PFY) measurements with no evidence of any IV-fold Al(III) coordination environment. This was in agreement with the solution measurements in which no significant Al dissolution from any of the Mg-Al-SO₄/CO₃ HTLCs was observed.

3.5 Adsorption and Solid State Phase Transformation Mechanisms (Al vs. Fe HTLCs): Environmental Implications

When combined, data from the XANES analyses relating to the local Fe, Mg, and Al redox and coordination environment of the reacted Mg(II)-Al(III)/Fe(III)-SO₄/CO₃ HTLCs, the bulk phase characterization (XRD and inert micro-Raman), and the solution analysis suggest two types of phase formation mechanisms occur upon the uptake of Fe(II)_(aq) (Fig. 10). In the case of the Fe-based HTLCs (Mg-Fe-SO₄/CO₃), phase formation occurs via adsorption of the Fe(II)_(aq) ions (and corresponding Mg(II)_(aq) release into solution) on the surface (detected via TEY-XANES) of the Fe-based HTLCs, resulting in layers of Fe(II)-Fe(III) layered double hydroxides in the form of GR (detected via inert micro-Raman and XANES). These Fe(II)-Fe(III) layer phases (i.e., GR) then transfer electrons between Fe(II)-Fe(III) HTLC sites to form the more thermodynamically stable MG phase not only at the surface but also within the bulk structure (as observed in bulk macro characterization techniques such as inert micro-Raman). To date, such processes have only been recorded for Fe(III) hydroxides-oxides.^{30-32, 36, 79-83}

For Fe(III) hydroxides-oxides, a hypothesized electron transfer and atom exchange (ETAE) between the Fe(II)_(aq) ions and the surface of the Fe(III) hydroxide-oxide solids (in our case, Mg-Fe-SO₄/CO₃ HTLCs) promotes their recrystallization into more crystalline and thermodynamically stable Fe(III)-Fe(III)/Fe(III)-Fe(II) phases (in our case, Fe(II)-Fe(III)-Mg(II)-Fe(III)/Al(III)-SO₄/CO₃), such as GR, MG, LP, GT, and FH.^{30-32, 36, 79-83}

In the case of the Al-based HTLCs (Mg-Al-SO₄/CO₃), the phase formation occurs via Fe(II)_(aq) adsorption, likely as double hydroxyl layers of Fe(II)-Fe(III) (i.e., GR) and/or Fe(II)-Al(III)^{37, 38} layered double hydroxides on the surface of the reacted Mg-Al-SO₄/CO₃ HTLCs. These surface layers of Fe(II)-Fe(III) layered double hydroxides (as GR, detected via inert micro-Raman and XANES) then transform to the more thermodynamically stable MG phase. In this case, because Al(III) is not a readily redox sensitive element (such as Fe(III)), the ETAE between the Fe(II)_(aq) ions and the surface of the Mg-Al-SO₄/CO₃ HTLC does not proceed throughout the bulk and is restricted to the surface deposited Fe(II)-Fe(III) and/or Fe(II)-Al(III) species.

Under the conditions considered, the formation of secondary Fe(II)-Fe(III)/Al(III)-SO₄/CO₃ HTLC-like phases form as Fe(II)_(aq) reacts with Mg(II)-Al(III)/Fe(III)-SO₄/CO₃ HTLC solids. The findings herein suggest two types of formation phase mechanisms via Fe(II)_(aq) uptake. Fe(II)_(aq) removal and precipitation is fast (~99% removal in day 1), and the capacity for

Fe(II) sorption is not limited by the available reactive surface sites as is the case for Fe(III)/Al(III)-oxy/hydroxides. The only exception to this was observed for the MgAlSO₄ at a target pH of 8 and 10 mM Fe(II)_(aq). As such, the formation of Fe(II)-Fe(III)/Al(III)-SO₄/CO₃ HTLC-like phases will not only affect either Fe(II) speciation and its solubility or, more importantly, retention and speciation of divalent metals (e.g., Zn, and Ni) as well as contaminants (As, Se, Mo, Ni, U) present (e.g., on Mg(II)-Al(III)/Fe(III)-SO₄/CO₃ HTLC solids).^{19-22, 24, 25, 84} It is well documented⁸⁵⁻⁸⁹ that Fe(II)/Fe(III) double layer hydroxide species such as GR (fougerite) and other Fe(II)-containing phases such as siderite (FeCO₃) can have an effect on the retention and valency of redox sensitive contaminants (e.g., As(V), Cr(VI), and Se(VI)) in the environment. As a result, we can infer that the GR phases formed from our Mg(II)-Al(III)/Fe(III)-SO₄/CO₃ HTLC substrates may also exhibit some type of valency reactivity of redox sensitive contaminants. To date, only controls on geochemical and environmentally important elements of concern (e.g., As) by Fe(III)-oxy/hydroxide (e.g., ferrihydrite, goethite, hematite) or Al(III)-oxy/hydroxides under anoxic abiotic (via Fe(II)_(aq) reductive dissolution have been reported. However, this study provides evidence for the first time of: (1) the abiotic (via Fe(II)_(aq)) anoxic reductive dissolution of Mg(II)-Al(III)/Fe(III)-SO₄/CO₃ HTLCs, (2) unrecognized secondary Fe(II)-Al(III)/Fe(III)-SO₄/CO₃ mineral phase formation mechanisms, and (3) GR and MG formation from non Fe-oxide/hydroxide substrates. These mechanisms are dependent upon the metal HTLC substrate (Al vs. Fe) that may in turn strongly influence the biogeochemical cycling of Fe and trace metal(loid)s in (periodically) suboxic and anoxic geochemical systems. Something that remains to be investigated is how the presence of adsorbed ions of elements of concern (e.g., AsO₄, MoO₄) on HTLCs affects the behavior observed here for a “clean” surface (no adsorbed elements of concern). For example, the presence of As on Fe(III)-oxy/hydroxide (e.g., ferrihydrite, goethite, hematite) and/or Al(III)-doped Fe(III)-oxy/hydroxide inhibits phase transformation and crystallization to more thermodynamic stable phases^{30, 31, 35, 42, 90-94}. However, no such data exist for Mg(II)-Al(III)/Fe(III)-SO₄/CO₃ HTLCs.

Acknowledgements

Financial support was provided by Cameco Corporation and the Natural Sciences and Engineering Research Council of Canada (NSERC) through a Senior Industrial Research Chair to MJH. Assistance received from F. Nelson, J. Fan, J. Lin, and T. Bonli (Geological Sciences) and the SGM/CLS staff (T. Regier, J. Dynes, and D. Chevrier) is kindly acknowledged.

Notes and references

- ^a Department of Geological Sciences, University of Saskatchewan, 114 Science Place, Saskatoon, Saskatchewan, S7N 5E2, Canada; E-mail: mag346@mail.usask.ca; Tel: 1-306-2616246
- ^b Department of Chemistry, University of Montreal, C.P. 6128, Succursale Centre-ville, Montreal, Quebec, H3C 3J7, Canada

† Electronic Supplementary Information (ESI) available: solid elemental composition and analysis of initial materials before reaction, tables summarizing element release and percentages of X element (X = Fe or

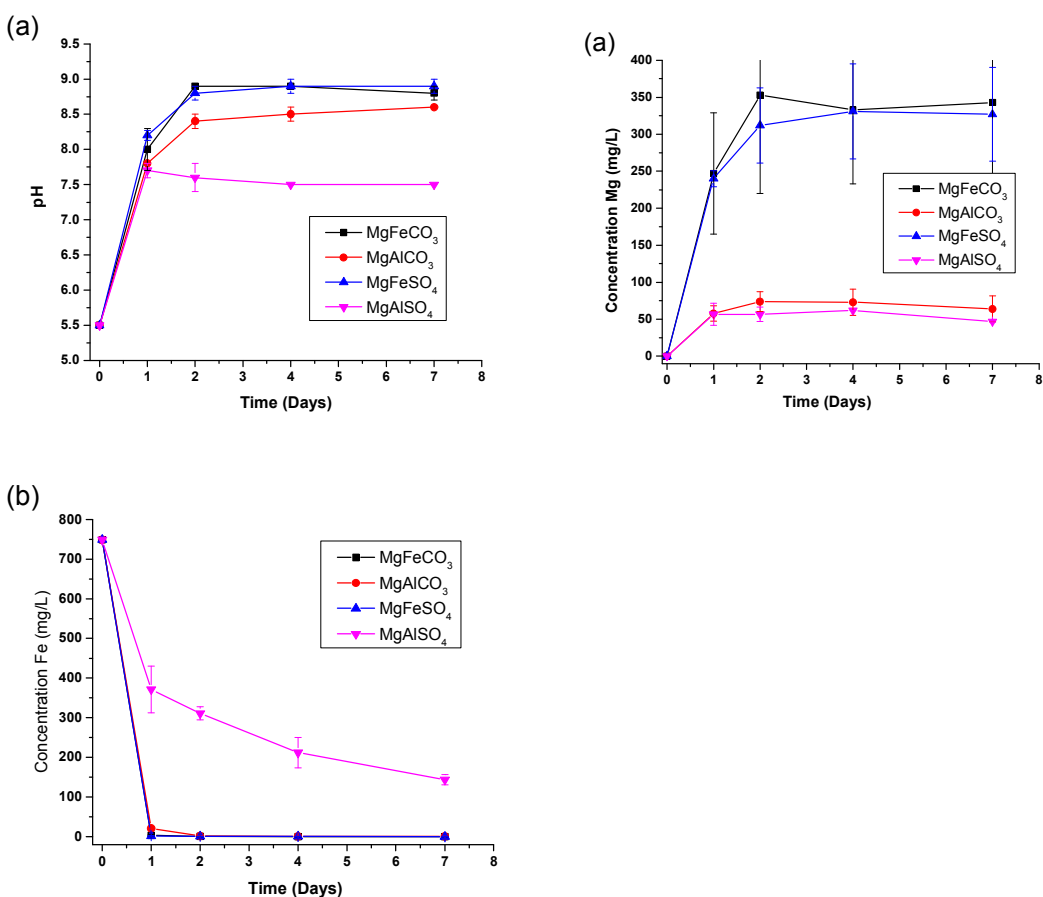
Mg) remaining in solution, individual test data, and phase transformation summary observed for all the reaction conditions. XRD, inert XANES, and inert micro-Raman data for selective samples discussed in the text are also presented herein. See DOI: 10.1039/b000000x/

1. F. Cavani, F. Trifirò and A. Vaccari, *Catal. Today*, 1991, **11**, 173.
2. C. Forano, T. Hibino, F. Leroux and C. Taviot-Gueho, Layered double hydroxides, in: F. Bergaya, B.K.G. Theng, G. Lagaly (Eds.), *Handbook of Clay Science*, Elsevier Ltd., 2006, pp. 1021.
3. R. L. Frost, A. W. Musumeci, J. T. Klopogge, M. O. Adebajo and W. N. Martens, *J. Raman Spectrosc.*, 2006, **37**, 733.
4. B. Grégoire, C. Ruby and C. Carteret, *Dalton Trans.*, 2013, **42**, 15687.
5. W. Li, K. J. T. Livi, W. Xu, M. G. Siebecker, Y. Wang, B. L. Phillips and D. L. Sparks., *Environ. Sci. Technol.*, 2012, **46**, 11670.
6. C. A. Johnson and F. P. Glasser, *Clays Clay Miner.*, 2003, **51**, 1.
7. P. J. Sideris, U. G. Nielsen, Z. Gan and C. P. Grey, *Science*, 2008, **321**, 113.
8. K. Rozov, U. Berner, C. Taviot-Gueho, F. Leroux, G. Renaudin, D. Kulik and L. W. Diamond, *Cem. Concr. Res.*, 2010, **40**, 1248.
9. S. Paikaray and M. J. Hendry, *Appl. Surf. Sci.*, 2012, **263**, 633.
10. Q. Wang and D. O'Hare, *Chem. Rev.*, 2012, **112**, 4124.
11. H. F. W. Taylor, *Mineral. Mag.*, 1973, **39**, 377.
12. M. R. Sturgeon, M. H. O'Brien, P. N. Ciesielski, R. Katahira, J. S. Kruger, S. C. Chmely, J. Hamlin, K. Lawrence, G. B. Hunsinger, T. D. Foust, R. M. Baldwin, M. J. Bidy and G. T. Beckham, *Green Chem.*, 2014, **16**, 824.
13. D. P. Debecker, E. M. Gaigneaux and G. Busca, *Chem.-Eur. J.*, 2009, **15**, 3920.
14. B. F. Sels, D. E. De Vos, M. Buntinx, F. Pierard, A. Kirsch-De Mesmaeker and P. A. Jacobs, *Nature*, 1999, **400**, 855.
15. B. F. Sels, D. E. De Vos and P. A. Jacobs, *Catal. Rev. Sci. Eng.*, 2001, **43**, 443.
16. L. Yang, Z. Shahrivari, P. K. T. Liu, M. Sahimi and T. T. Tsotsis, *Ind. Eng. Chem. Res.*, 2005, **44**, 6804.
17. L. Cochechi, R. Pode, E. Popovici, E. Dvininov and A. Iovi, *Environ. Eng. Manag. J.*, 2009, **8**, 865.
18. R. Liu, R. L. Frost and W. N. Martens, *Water Res.*, 2009, **43**, 1323.
19. K. Grover, S. Komarneni and H. Katsuki, *Water Res.*, 2009, **43**, 884.
20. T. Türk, İ. Alp and H. Deveci, *J. Hazard. Mater.*, 2009, **171**, 665.
21. G. B. Douglas, L. A. Wendling, R. Pleysier and M. G. Trefry, *Mine Water Environ.*, 2010, **29**, 108.
22. M. A. Gomez, M. J. Hendry, J. Koshinsky, J. Essilfie-Dughan, S. Paikaray and J. Chen, *Environ. Sci. Technol.*, 2013, **47**, 7883.
23. S. Nishimura, A. Tagaki and K. Ebitani, *Green Chem.*, 2013, **15**, 2026.
24. G. Douglas, M. Shackelton and P. Woods, *Appl. Geochem.*, 2014, **42**, 27.
25. S. Paikaray, M. J. Hendry and J. Essilfie-Dughan, *Chem. Geol.*, 2013, **345**, 130.
26. M. Jobbagy, M. A. Blesa and A. E. Regazzoni, *J. Colloid Interface Sci.*, 2007, **309**, 72.
27. S. Paikaray and M. J. Hendry, *Appl. Clay Sci.*, 2014, **88-89**, 111.
28. Y. Yang, X. Zhao, Y. Zhu and F. Zhang, *Chem. Mater.*, 2012, **24**, 81.
29. S. Paikaray, M. A. Gomez, M. J. Hendry and J. Essilfie-Dughan, *RSC Adv.*, 2014, submitted.
30. C. M. Hansel, S. G. Benner and S. Fendorf, *Environ. Sci. Technol.*, 2005, **39**, 7147.
31. L. Yang, C. I. Steefel, M. A. Marcus and J. R. Bargar, *Environ. Sci. Technol.*, 2010, **44**, 5469.
32. R. M. Handler, B. L. Beard, C. M. Johnson and M. M. Scherer, *Environ. Sci. Technol.*, 2009, **43**, 1102.
33. D. E. Latta, J. E. Bachman and M. M. Scherer, *Environ. Sci. Technol.*, 2012, **46** 10614.
34. J. A. Frierdich and J. G. Catalano, *Environ. Sci. Technol.*, 2012b, **46** 1519.
35. M. A. Gomez, M. J. Hendry, A. Hossain, S. Das and S. Elouatik, *RSC Adv.*, 2013, **3**, 25812.
36. G. C. Murray and D. Hesterberg, *Soil Sci. Soc. Am. J.*, 2006, **70**, 1318.
37. E. J. Elzinga, *Environ. Sci. Technol.*, 2012, **46**, 4894.
38. Y. Zhu and E. J. Elzinga, *Environ. Sci. Technol.*, 2014, **46**, 4894.
39. R. M. Cornell and U. Schwertmann, Cation substitution. In *The iron oxides: structure, properties, reactions, occurrence and uses*; VCH: Weinheim, Germany, 1996; pp 35-52.

40. J. Pérez-Ramírez, S. Abelló and N. M. van der Pers, *Chem.-Eur. J.*, 2007, **13**, 870-878.
41. Y. Liu, D. Ma, R. A. Blackley, W. Zhou, X. Han and X. Bao, *J. Phys. Chem. C*, 2008, **112**, 4124.
42. H. D. Pedersen, D. Postma and R. Jakobsen, *Geochim. Cosmochim. Acta.*, 2006, **70**, 4116.
43. US-EPA, 1997, Developments for In Situ Treatment of Metal Contaminated Soils. <http://www.clu-in.org/download/remed/metals2.pdf>.
44. D. L. Bish and S. J. Chipera, 1995. Accuracy in quantitative X-ray powder diffraction analyses, *Advances in X-ray Analysis* v. 38, (Predecki, P., et al., eds.), Plenum Pub.Co., p. 47-57.
45. I. A. M. Ahmed, L. G. Benning, G. Kakonyi, A. D. Sumoondur, N. J. Terrill and S. Shaw, *Langmuir*, 2010, **26**, 6593.
46. L. Legrand, G. Sagon, S. Lecomte, A. Chausse and R. Messina, *Corros. Sci.*, 2001, **43**, 1739.
47. L. Mazzetti and P. J. Thistlethwaite, *J. Raman Spectrosc.*, 2002, **33**, 104.
48. M. L. Franquelo, A. Duran, L. K. Herrera, M. C. Jimenez de Haro and J. L. Perez-Rodriguez, *J. Mol. Struct.*, 2009, **924-926**, 404.
49. T. Regier, J. Paulsen, G. Wright, I. Coulthard, K. Tan, T. K. Sham and R. I. R. Blyth, *AIP Conf. Proc.*, 2007, **879**, 473-476.
50. A. Gloter, M. Zbinden, F. Guyot, F. Gaill and C. Colliex, *Earth Planet. Sci. Lett.*, 2004, **222**, 947.
51. T. H. Yoon, S. B. Johnson, K. Benzerara, C. S. Doyle, T. Tylliszczak, D. K. Shuh and G. E. Brown, *Langmuir*, 2004, **20**, 10361.
52. H. Aritani, H. Yamada, T. Nishio, T. Shiono, S. Imamura, M. Kudo, S. Hasegawa, T. Tanaka and S. Yoshida, *J. Phys. Chem. B*, 2000, **104**, 10133.
53. J. C. A. A. Roelofs, J. A. van Bokhoven, A. J. van Dillen, J. W. Geus and K. P. de Jong, *Chem. Eur. J.*, 2002, **8**, 5571.
54. J. A. van Bokhoven, J. C. A. A. Roelofs, K. P. de Jong and D. C. Koningsberger, *Chem. Eur. J.*, 2001, **7**, 1258.
55. C. S. Doyle, S. J. Traina, H. Ruppert, T. Kendelewicz, J. J. Rehr and G. E. Brown, Jr, *J. Synchrotron Rad.*, 1999, **6**, 621.
56. K.-i. Shimizu, Y. Kato, H. Yoshida, A. Satsuma, T. Hattori and T. Yoshida, *Chem. Commun.*, 1999, 1681.
57. C. Pantke, M. Obst, K. Benzerara, G. Morin, G. Ona-Nguema, U. Dippon and A. Kappler, *Environ. Sci. Technol.*, 2012, **46**, 1439.
58. D. Peak and T. Regier, *Environ. Sci. Technol.*, 2012, **46**, 3163.
59. F. M. F. de Groot, J. C. Fuggle, B. T. Thole and G. A. Sawatzky, *Phys. Rev. B: Condens. Matter*, 1990, **42**, 5459.
60. F. M. F. de Groot, *Coord. Chem. Rev.*, 2005, **249**, 31.
61. E. Otero, R. G. Wilks, T. Regier, R. I. R. Blyth, A. Moewes and S. G. Urquhart, *J. Phys. Chem. A.*, 2008, **112**, 624.
62. E. C. Todd, D. M. Sherman and J. A. Purton, *Geochim. Cosmochim. Acta.*, 2003, **67**, 2137.
63. J. P. Crocombette, M. Pollal, F. Jollet, N. Thromat and M. Gautier-Soyer, *Phys. Rev. B*, 1995, **52**, 3143.
64. N. Hollmann, M. Valldor, H. Wu, Z. Hu, N. Qureshi, T. Willers, Y.-Y. Chin, J. C. Cezar, A. Tanaka, N. B. Brookes and L. H. Tjeng, *Phys. Rev. B*, 2011, **83**, 180405.
65. J. Stöhr, *NEXAFS Spectroscopy*, Springer: Berlin, 1992.
66. P. Kruger, *Phys. Rev. B.*, 2010, **81**, 12512.
67. G. A. Jenner, H. P. Longerich, S. E. Jackson and B. J. Fryer, *Chem. Geol.*, 1990, **83**, 133.
68. H. P. Longerich, G. Jenner, B. Fryer and S. Jackson, *Chem. Geol.*, 1990, **83**, 105.
69. A. Sumoondur, S. Shaw, I. Ahmed and L. G. Benning, *Mineral. Mag.*, 2008, **72**, 201.
70. M. Usman, K. Hanna, M. Abdelmoula, A. Zegeye, P. Faure and C. Ruby, *Appl. Clay Sci.*, 2012, **64**, 38.
71. W. Rudolph, M. H. Brooker and P. R. Tremaine, *J. Solution Chem.*, 1997, **26**, 757.
72. N. Huse, T. K. Kim, L. Jamula, J. K. McCusker, F. M. F. de Groot and R. W. Schoenlein, *J. Am. Chem. Soc.*, 2010, **132**, 6809.
73. P. A. van Aken and S. Lauterbach, *Phys. Chem. Miner.*, 2003, **30**, 469.
74. M. Bellotto, B. Rebours, O. Clause, J. Lynch, D. Bazin and E. Elkaïm, *J. Phys. Chem.*, 1996, **100**, 8527.
75. S. J. Mills, A. G. Christy, J.-M. R. Génin, T. Kameda and F. Colombo, *Mineral. Mag.*, 2012, **76**, 1289.
76. L. Simon, M. François, P. Refait, G. Renaudin, M. Lelaurain and J.-M. R. Génin, *Solid State Sci.*, 2003, **5**, 327.
77. R. Allman, *Acta Cryst.*, 1968, **B24**, 972.

78. C. Ruby, C. Upadhyay, A. Gehin, G. Onanguema and J. M. R. Genin, *Environ. Sci. Technol.*, 2006, **40**, 4696.
79. J. R. Lloyd, *FEMS Microbiol. Rev.*, 2003, **27**, 411.
80. R. Schaetzl and S. Anderson, *Soils: Genesis and Geomorphology*, Cambridge University Press, Cambridge, UK, 2005, p. 817.
81. N. R. Posth, F. Hegler, K. O. Konhauser and A. Kappler, *Nat. Geosci.*, 2008, **1**, 703.
82. D. A. Lipson, M. Jha, T. K. Raab and W. C. Oechel, *J. Geophys. Res.*, 2010, **115**, 2156.
83. C. A. Gorski and M. M. Scherer, Fe²⁺ sorption at the Fe oxide-water interface: A revised conceptual framework. In *Aquatic Redox Chemistry*; American Chemical Society: 2011; Vol. 1071, pp 315–343.
84. R. L. Frost, W. N. Martens and R. Liu, *Water Res.*, 2009, **43**, 1323.
85. A. G. B. Williams and M. M. Scherer, *Environ. Sci. Technol.*, 2001, **35**, 3488.
86. J. M. R. Genin, P. Refait, G. Bourrie, M. Abdelmoula and F. Trolard, *Appl. Geochem.*, 2001, **16**, 559.
87. S. R. Randall, D. M. Sherman and K. V. Ragnarsdottir, *Geochim. Cosmochim. Acta.*, 2001, **65**, 1015.
88. J. Jonsson and D. M. Sherman, *Chem. Geol.*, 2008, **255** 173.
89. Y. Wang, G. Morin, G. Ona-Nguema, F. Juillot, F. Guyot, G. Calas and G. E. Brown, *Environ. Sci. Technol.*, 2010, **44**, 109.
90. J. J. Erbs, T. S. Berquó, B. C. Reinsch, G. V. Lowry, S. K. Banerjee and R. L. Penn, *Geochim. Cosmochim. Acta*, 2010, **74**, 3382.
91. Y. Masue-Slowey, R. H. Loeppert and S. Fendorf, *Geochim. Cosmochim. Acta*, 2011, **75**, 870.
92. H. Liu, P. Li, M. Zhu, Y. Wei and Y. Sun, *J. Solid State Chem.*, 2007, **180**, 2121.
93. H. Liu, P. Li, B. Lu, Y. Wei and Y. Sun, *J. Solid State Chem.*, 2009, **182**, 1767.
94. J. Jang, B. A. Dempsey, G. L. Catchen and W. D. Burgos, *Colloids Surf., A*, 2003, **221**, 55.

Figure 1. Profiles of pH and leachability of the total aqueous Fe and Mg as a function of time for tests conducted at pH 8 for 7 days with 10 mM Fe(II)_(aq). Time 0 days represents conditions before Mg(II)-Al(III)/Fe(III)-CO₃/SO₄ HTLC solids were added. Concentration units for (Fe) and (Mg) are mg/L. Values reported are the average and standard deviation (error bars) of duplicate tests. Individual test data are provided in the supplementary information.



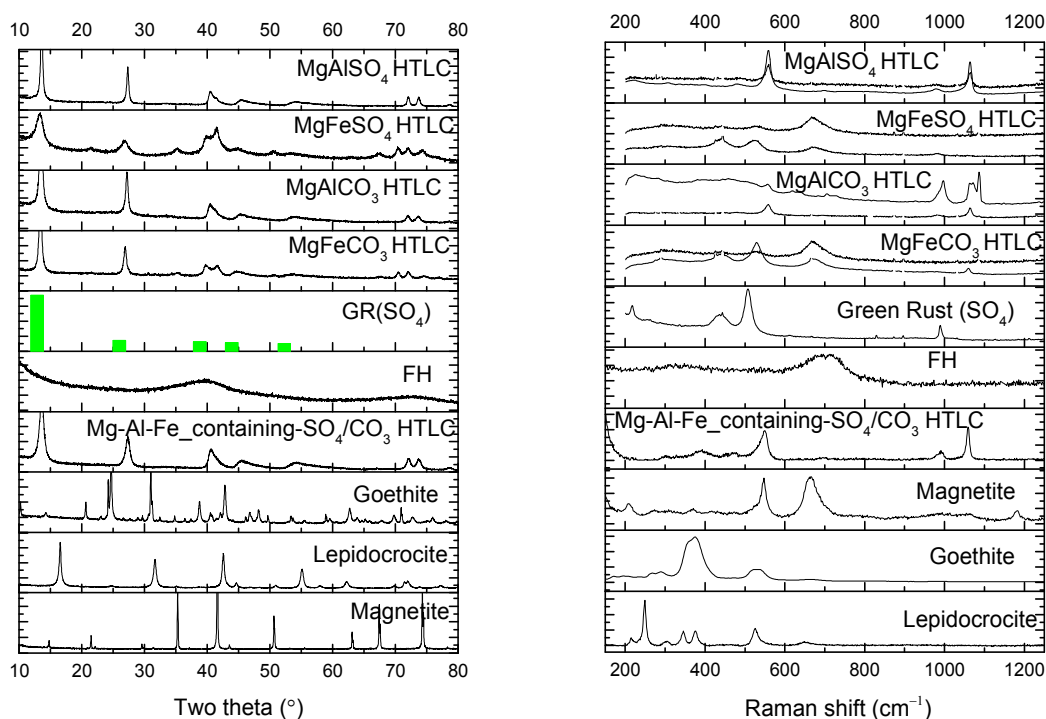
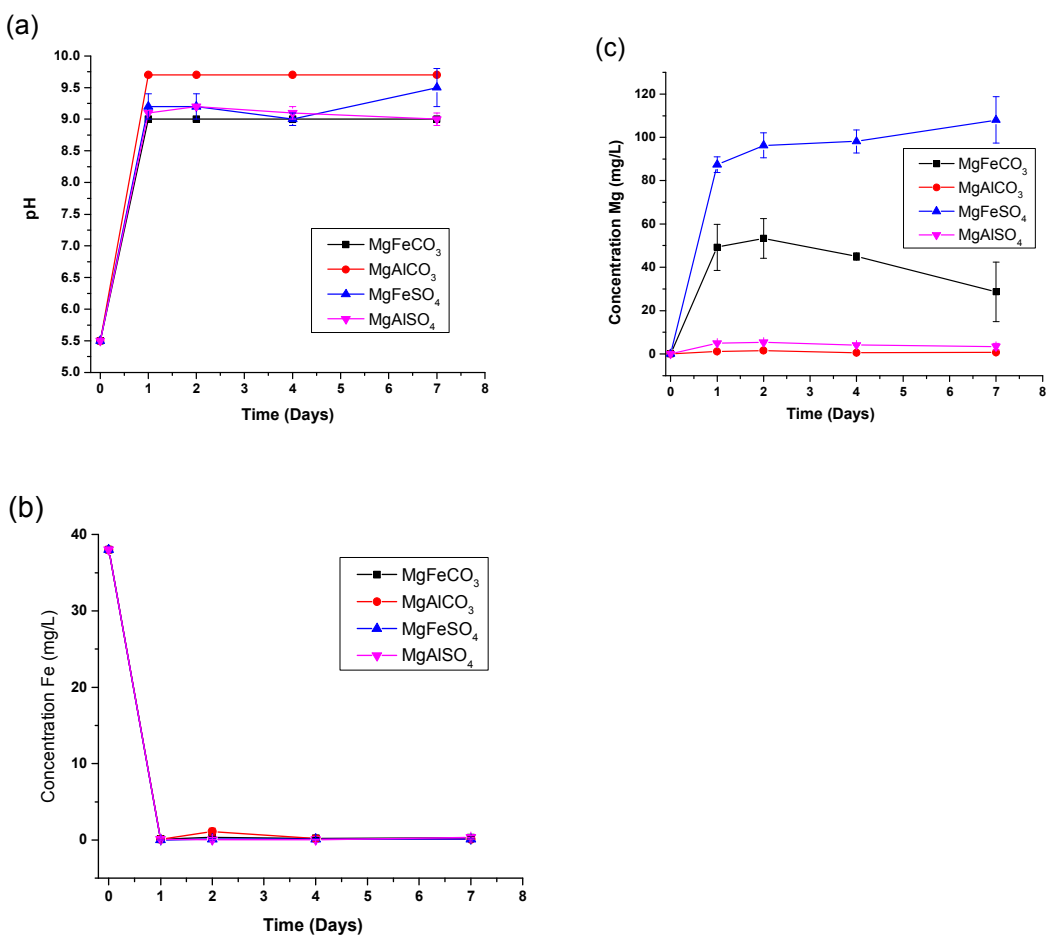


Figure 2. Powder X-ray diffraction spectra (left) and inert micro-Raman spectra (right) of Mg(II)-Al(III)/Fe(III)-CO₃/SO₄ solid products reacted at a target pH of 8 for 7 days with 10 mM Fe(II)_(aq). Spectra of relevant standard materials (LP, GT, MG, FH, GR(SO₄), Mg(II)-Al(III)-Fe(III) containing-SO₄/CO₃) are shown for comparison. For each reacted sample, two Raman spectra are presented to show the mixture of phases found in the reacted sample. This figure shows the observed bulk phase changes that occur upon the adsorption of Fe(II)_(aq) ions on the Mg(II)-Al(III)/Fe(III) CO₃/SO₄ HTLC substrates at the noted reacting condition.

Figure 3. Profiles of pH and leachability of the total aqueous Fe and Mg as a function of time for tests conducted at pH 8 for 7 days with 0.5 mM Fe(II)_(aq). Time 0 days represents conditions before Mg(II)-Al(III)/Fe(III)-CO₃/SO₄ HTLC solids were added. Concentration units for (Fe) and (Mg) are mg/L. Values reported are the average and standard deviation (error bars) of duplicate tests. Individual test data are provided in the supplementary information.



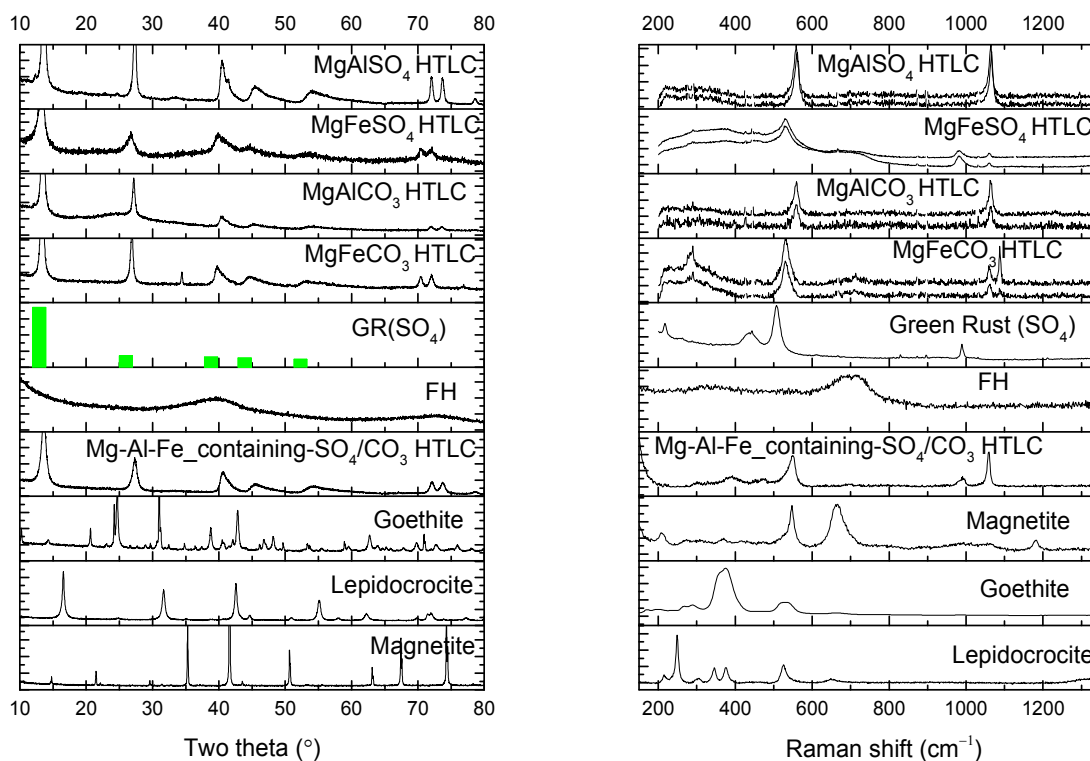
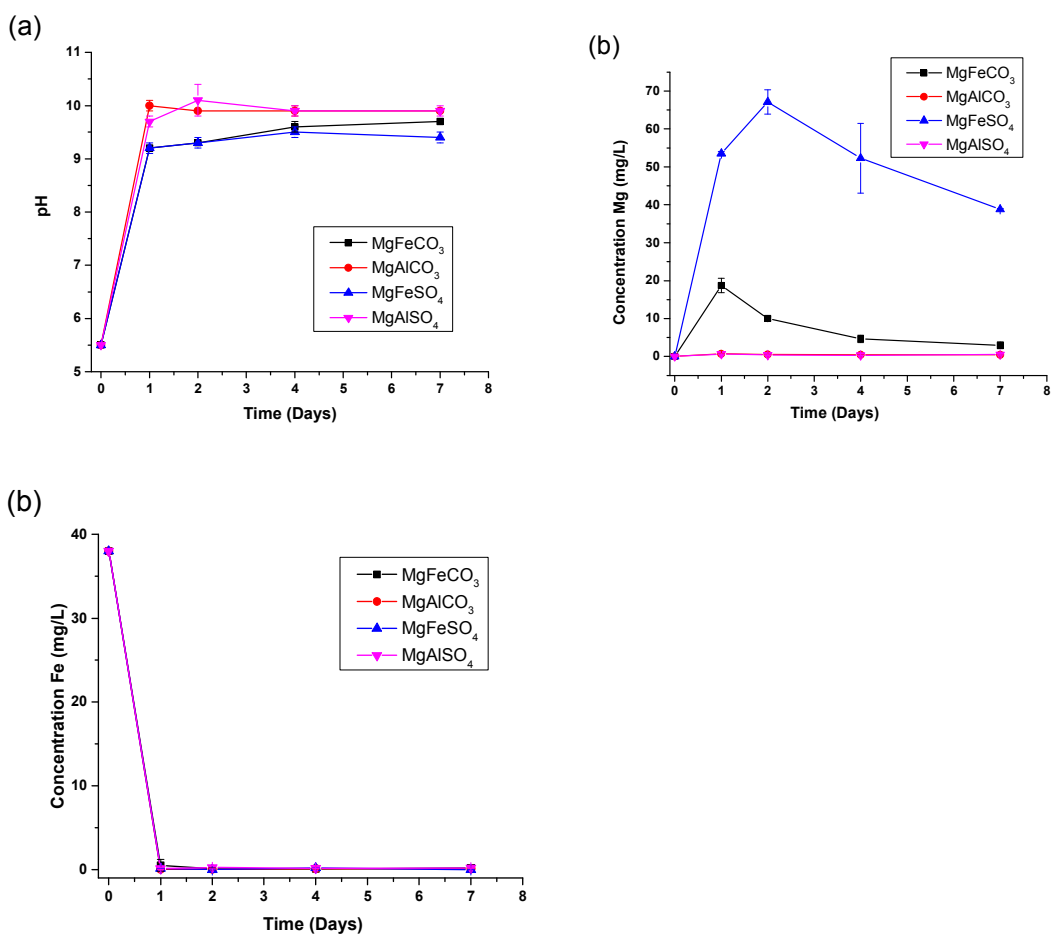


Figure 4. Powder X-ray diffraction spectra (left) and inert micro-Raman spectra (right) of Mg(II)-Al(III)/Fe(III)-CO₃/SO₄ solid products reacted at a target pH of 8 for 7 days with 0.5 mM Fe(II)_(aq). Spectra of relevant standard materials (LP, GT, MG, FH, GR(SO₄), Mg(II)-Al(III)-Fe(III) containing-SO₄/CO₃) are shown for comparison. For each reacted sample, two Raman spectra are presented to show the mixture of phases found in the reacted sample. This figure shows the observed bulk phase changes that occur upon the adsorption of Fe(II)_(aq) ions on the Mg(II)-Al(III)/Fe(III) CO₃/SO₄ HTLC substrates at the noted reacting condition.

Figure 5. Profiles of pH and leachability of the total aqueous Fe and Mg as a function of time for tests conducted at pH 10 for 7 days with 0.5 mM Fe(II)_(aq). Time 0 days represents conditions before Mg(II)-Al(III)/Fe(III)-CO₃/SO₄ HTLC solids were added. Concentration units for (Fe) and (Mg) are mg/L. Values reported are the average and standard deviation (error bars) of duplicate tests. Individual test data are provided in the supplementary information.



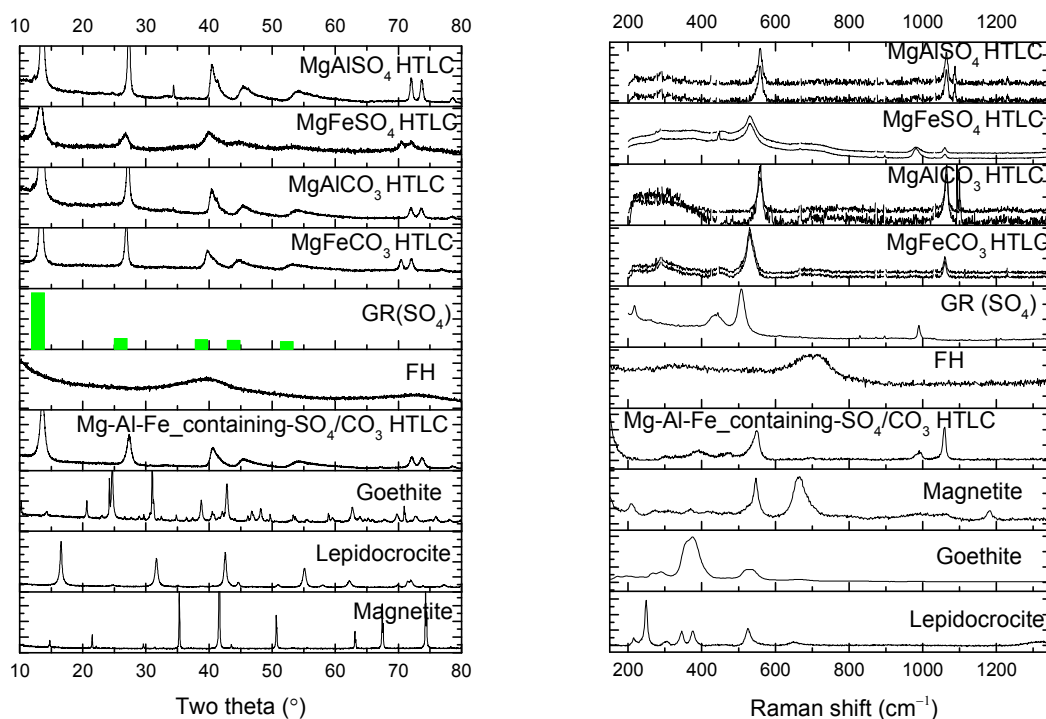


Figure 6. Powder X-ray diffraction spectra (left) and inert micro-Raman spectra (right) of Mg(II)-Al(III)/Fe(III)-CO₃/SO₄ HTLCs reacted solids at a target pH of 10 for 7 days with 0.5 mM Fe(II)_(aq). Spectra of relevant standard materials (LP, GT, MG, FH, GR(SO₄), Mg(II)-Al(III)-Fe(III) containing-SO₄/CO₃) are shown for comparison. For each reacted sample, two Raman spectra are presented to show the mixture of phases found in the reacted sample. This figure shows the observed bulk phase changes that occur upon the adsorption of Fe(II)_(aq) ions on the Mg(II)-Al(III)/Fe(III) CO₃/SO₄ HTLC substrates at the noted reacting condition.

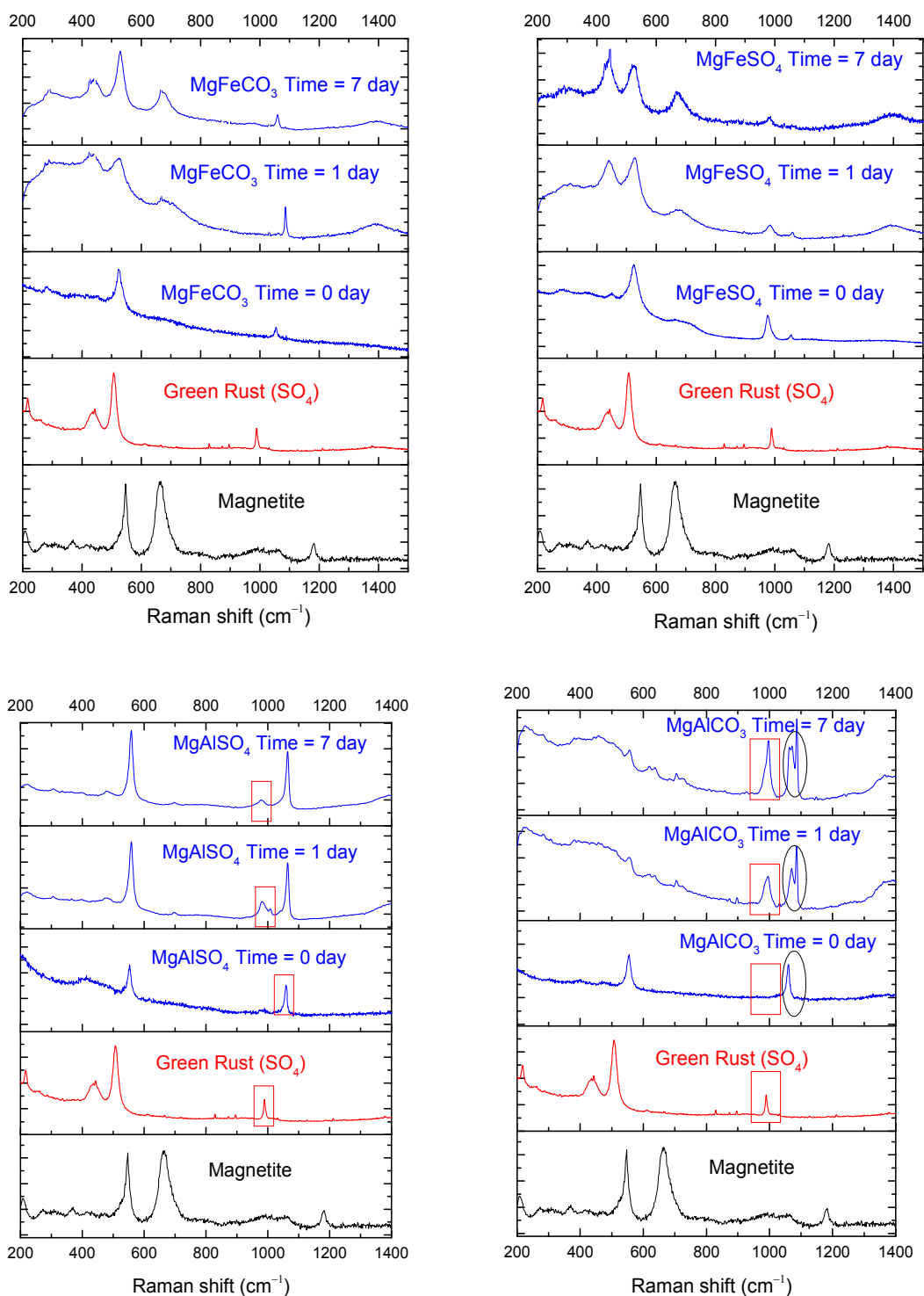


Fig 7. Inert micro-Raman spectra of the Mg(II)-Al(III)/Fe(III)-CO₃/SO₄ HTLCs reacted at a target pH of 8 for 0 days, 1 day, and 7 days with 10 mM Fe(II)_(aq) compared to standard green rust (SO₄) and magnetite. The squares and circles in the reacted Mg-Al-CO₃/SO₄ HTLCs highlight the sulfate and carbonate bands, respectively.

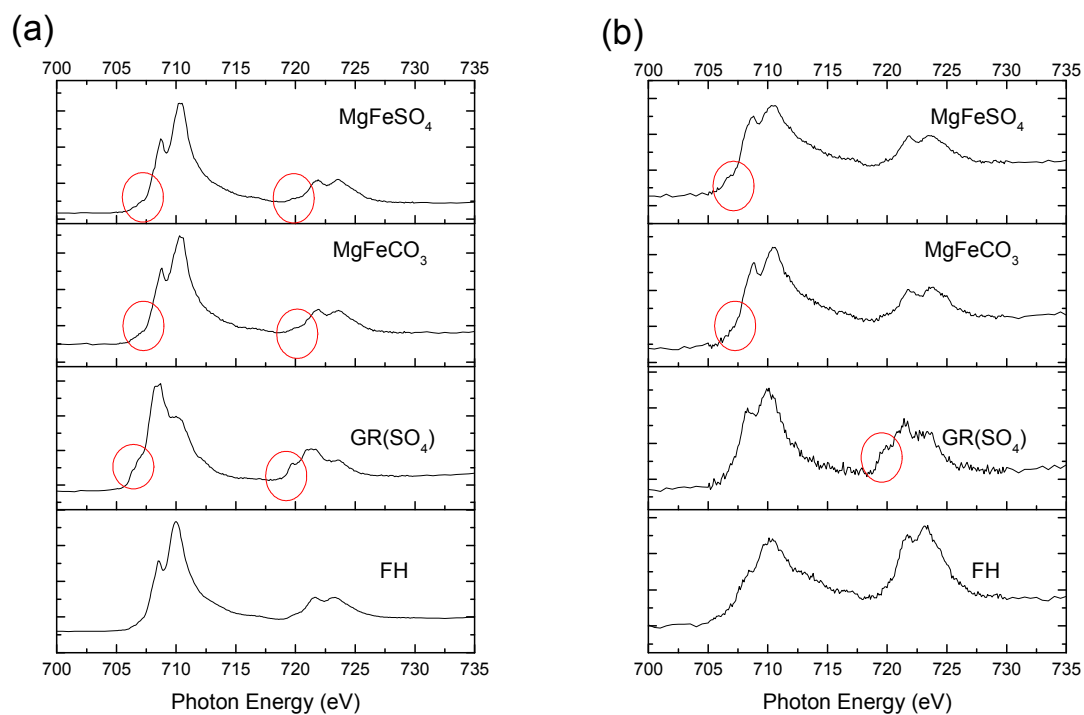


Fig 8. Fe L-edge (a) TEY (surface) and (b) PFY (bulk) spectra of the MgFeCO₃ and MgFeSO₄ HTLCs reacted at a target pH of 8 for 7 days with 10 mM Fe(II)_(aq) compared to standard green rust (GR) and ferrihydrite (FH).³⁵ The Fe(II) character of the reacted MgFeCO₃ and MgFeSO₄ HTLCs is highlighted by red circles. The energy scale presented in these spectra is relative.

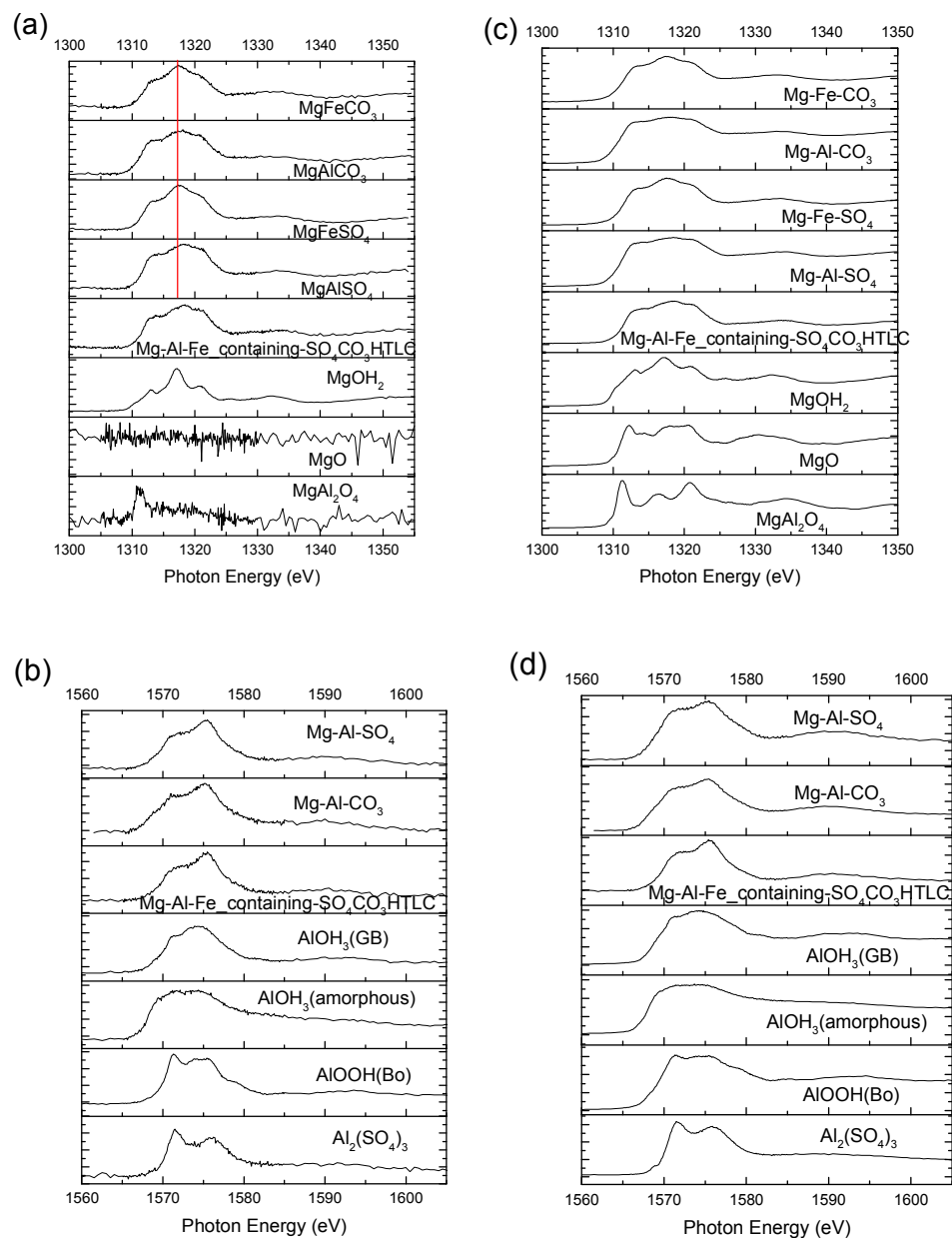


Fig 9. Mg and Al K-edge TEY (a and b, surface) and PFY (c and d, bulk) XANES spectra of the Mg(II)-Al(III)/Fe(III)-CO₃/SO₄ HTLCs reacted at a target pH of 8 for 7 days with 10 mM Fe(II)_(aq) compared with standards: Mg(II)-Al(III)-Fe(III) containing-SO₄-CO₃ HTLC, MgO, MgOH₂ (brucite), MgAl₂O₄, Al₂(SO₄)₃, AlOOH (Bo: Boehmite), AlOH₃ (GB: Gibbsite), and AlOH₃ (amorphous). The energy scale presented in these spectra is relative.

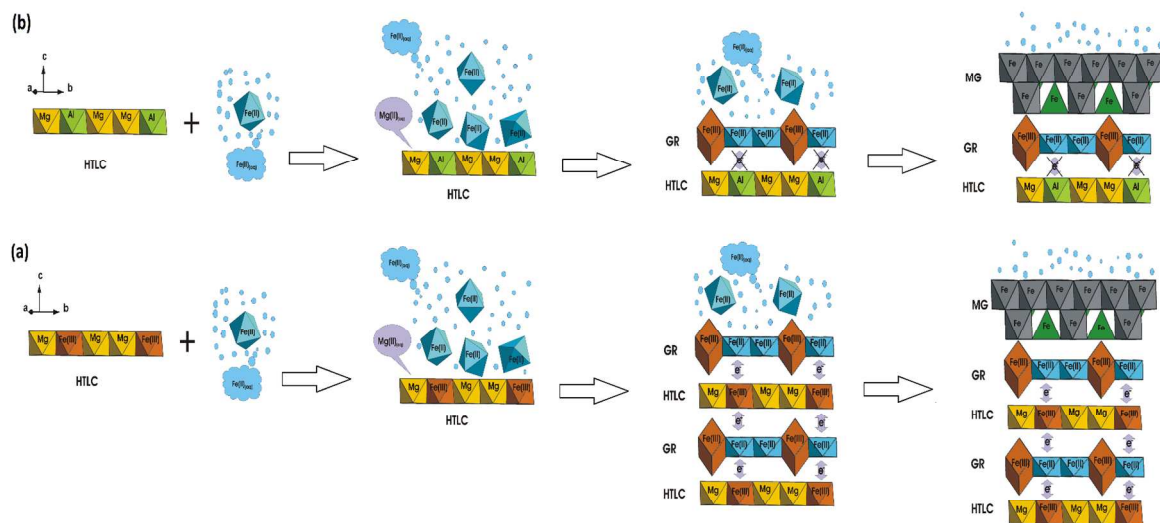
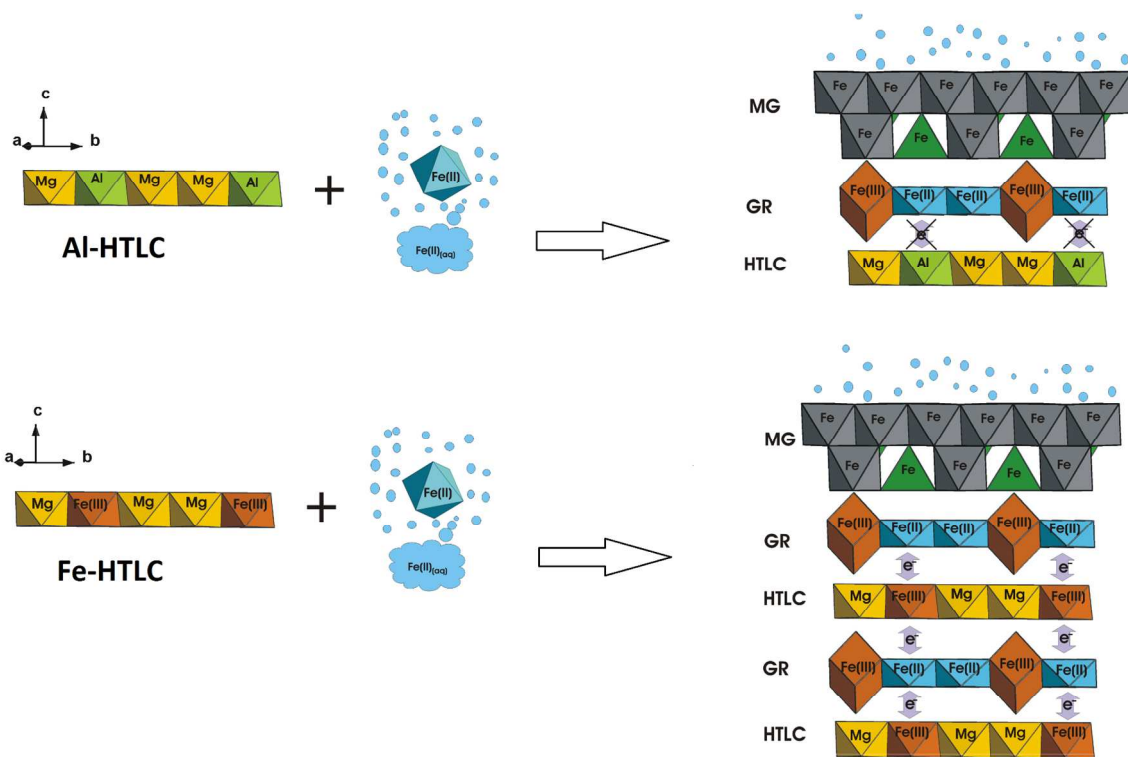


Fig 10. $\text{Fe(II)}_{(\text{aq})}$ uptake and phase transformation mechanisms of (a) $\text{Mg-Fe-SO}_4/\text{CO}_3$ and (b) $\text{Mg-Al-SO}_4/\text{CO}_3$ HTLCs under abiotic anoxic conditions. Although both cases have similar first adsorption steps and green rust (GR)/magnetite (MG) phase formation, electron transfer between the redox sensitive elements (Fe(III) vs. Al(III)) in the $\text{Mg(II)-Al(III)/Fe(III)-SO}_4/\text{CO}_3$ HTLCs ultimately determines whether phase transformation occurs only at the surface or deeper into the bulk. All $\text{Mg(II)-Al(III)/Fe(III)-SO}_4/\text{CO}_3$ HTLCs, GR, and MG structures depicted are from literature crystallographic data^{74,76-78} and for all cases the interlayer ions are omitted from the structures because they do not play a significant role in the mechanisms.



TOC Figure